

CERN/TH 95-333  
 Göteborg ITP 95-27  
 atom-ph/9601004  
 Christmas 1995

# Dynamics, Correlations and Phases of the Micromaser

Per Elmfors<sup>1,a)</sup>, Benny Lautrup<sup>2,a,b)</sup> and Bo-Sture Skagerstam<sup>3,c,d)</sup>

<sup>a)</sup> CERN, TH-Division, CH-1211 Geneva 23, Switzerland

<sup>b)</sup> CONNECT, The Niels Bohr Institute, Blegdamsvej 17,  
 DK-2100 Copenhagen, Denmark

<sup>c)</sup> Institute of Theoretical Physics, Chalmers University of Technology  
 and Göteborg University, S-412 96 Göteborg, Sweden

<sup>d)</sup> Department of Physics, University of Trondheim, N-7055 Dragvoll, Norway

## Abstract

The micromaser possesses a variety of dynamical phase transitions parametrized by the flux of atoms and the time-of-flight of the atom within the cavity. We discuss how these phases may be revealed to an observer outside the cavity using the long-time correlation length in the atomic beam. Some of the phase transitions are not reflected in the average excitation level of the outgoing atom, which is the commonly used observable. The correlation length is directly related to the leading eigenvalue of the time evolution operator, which we study in order to elucidate the phase structure. We find that as a function of the time-of-flight the transition from the thermal to the maser phase is characterized by a sharp peak in the correlation length. For longer times-of-flight there is a transition to a phase where the correlation length grows exponentially with the flux. We present a detailed numerical and analytical treatment of the different phases and discuss the physics behind them.

CERN/TH 95-333  
 Göteborg ITP 95-27  
 atom-ph/9601004  
 Christmas 1995

---

<sup>1</sup>email: elmfors@cern.ch

<sup>2</sup>email: lautrup@connect.nbi.dk

<sup>3</sup>email: tfebss@fy.chalmers.se

# Contents

<b>1</b>	<b>Introduction</b>	<b>1</b>
<b>2</b>	<b>Basic micromaser theory</b>	<b>2</b>
2.1	The Jaynes–Cummings Model . . . . .	3
2.2	Mixed states . . . . .	4
2.3	The lossless cavity . . . . .	7
2.4	The dissipative cavity . . . . .	7
2.5	The discrete master equation . . . . .	8
<b>3</b>	<b>Correlations</b>	<b>9</b>
3.1	Atomic beam observables . . . . .	10
3.2	Cavity observables . . . . .	11
3.3	Monte Carlo determination of correlation lengths . . . . .	13
3.4	Numerical calculation of correlation lengths . . . . .	14
<b>4</b>	<b>Analytic preliminaries</b>	<b>17</b>
4.1	Continuous master equation . . . . .	17
4.2	Relation to the discrete case . . . . .	18
4.3	The eigenvalue problem . . . . .	18
4.4	Effective potential . . . . .	21
4.5	Semicontinuous formulation . . . . .	21
4.6	Extrema of the continuous potential . . . . .	23
<b>5</b>	<b>Phase structure</b>	<b>25</b>
5.1	Empty cavity . . . . .	26
5.2	Thermal phase: $0 \leq \theta < 1$ . . . . .	27
5.3	First critical point: $\theta = 1$ . . . . .	28
5.4	Maser phase: $1 < \theta < \theta_1 \simeq 4.603$ . . . . .	29
5.5	Mean field calculation . . . . .	30
5.6	The first critical phase: $4.603 \simeq \theta_1 < \theta < \theta_2 \simeq 7.790$ . . . . .	33
<b>6</b>	<b>Effects of velocity fluctuations</b>	<b>38</b>
6.1	Revivals and prerevivals . . . . .	39
6.2	Phase diagram . . . . .	41
<b>7</b>	<b>Finite-flux effects</b>	<b>42</b>
7.1	Trapping states . . . . .	43
7.2	Thermal cavity revivals . . . . .	44
<b>8</b>	<b>Conclusions</b>	<b>46</b>
<b>A</b>	<b>Jaynes–Cummings with damping</b>	<b>48</b>
<b>B</b>	<b>Sum rule for the correlation lengths</b>	<b>50</b>
<b>C</b>	<b>Damping matrix</b>	<b>52</b>

# 1 Introduction

The highly idealized physical system of a single two-level atom in a superconducting cavity, interacting with a quantized single-mode electromagnetic field, has been experimentally realized in the micromaser [1]–[5] and microlaser systems [6]. Details and references to the literature can be found in e.g. the reviews [7]–[13]. In the absence of dissipation (and in the rotating wave approximation) the two-level atom and its interaction with the radiation field is well described by the Jaynes–Cummings (JC) Hamiltonian [14]. Since this model is exactly solvable it has played an important role in the development of modern quantum optics (for a recent account see e.g. Refs. [12, 13]). The JC model predicts non-classical phenomena, such as revivals of the initial excited state of the atom [15]–[20], experimental signs of which have been reported [21].

Correlation phenomena are important ingredients in the experimental and theoretical investigation of physical systems. Intensity correlations of light was e.g. used by Hanbury–Brown and Twiss [22] as a tool to determine the angular diameter of distant stars. The quantum theory of intensity correlations of light was later developed by Glauber [23]. These methods have a wide range of physical applications including investigation of the space-time evolution of high-energy particle and nuclei interactions [24, 25]. In the case of the micromaser we have recently suggested [26] that correlation measurements on atoms leaving the micromaser system can be used to infer properties of the quantum state of the radiation field in the cavity.

In this paper we present a detailed account of the role of long-time correlations in the outgoing atomic beam and their relation to the various phases of the micromaser system. Fluctuations in the number of atoms in the lower maser level for a fixed transit time  $\tau$  is known to be related to the photon-number statistics [27]–[30]. The experimental results of [31] are clearly consistent with the appearance of non-classical, sub-Poissonian statistics of the radiation field, and exhibit the intricate correlation between the atomic beam and the quantum state of the cavity. Related work on characteristic statistical properties of the beam of atoms emerging from the micromaser cavity may be found in Ref. [32].

The paper is organized as follows. In Section 2 we discuss the standard theoretical framework for the micromaser and introduce some new notation. A general discussion of long-time correlations is given in Section 3, where we also determine the correlation length numerically. Before entering the analytic investigation of the phase structure we introduce some useful concepts in Section 4 and discuss the eigenvalue problem for the correlation length. The heart of the paper lies in Section 5, where details of the different phases are analysed. In Section 6 we study effects related to the finite spread in atomic velocities. The phase boundaries are defined in the limit of an infinite flux of atoms, but there are several interesting effects related to finite fluxes as well. We discuss these issues in Section 7. Finally we summarize our results in Section 8.

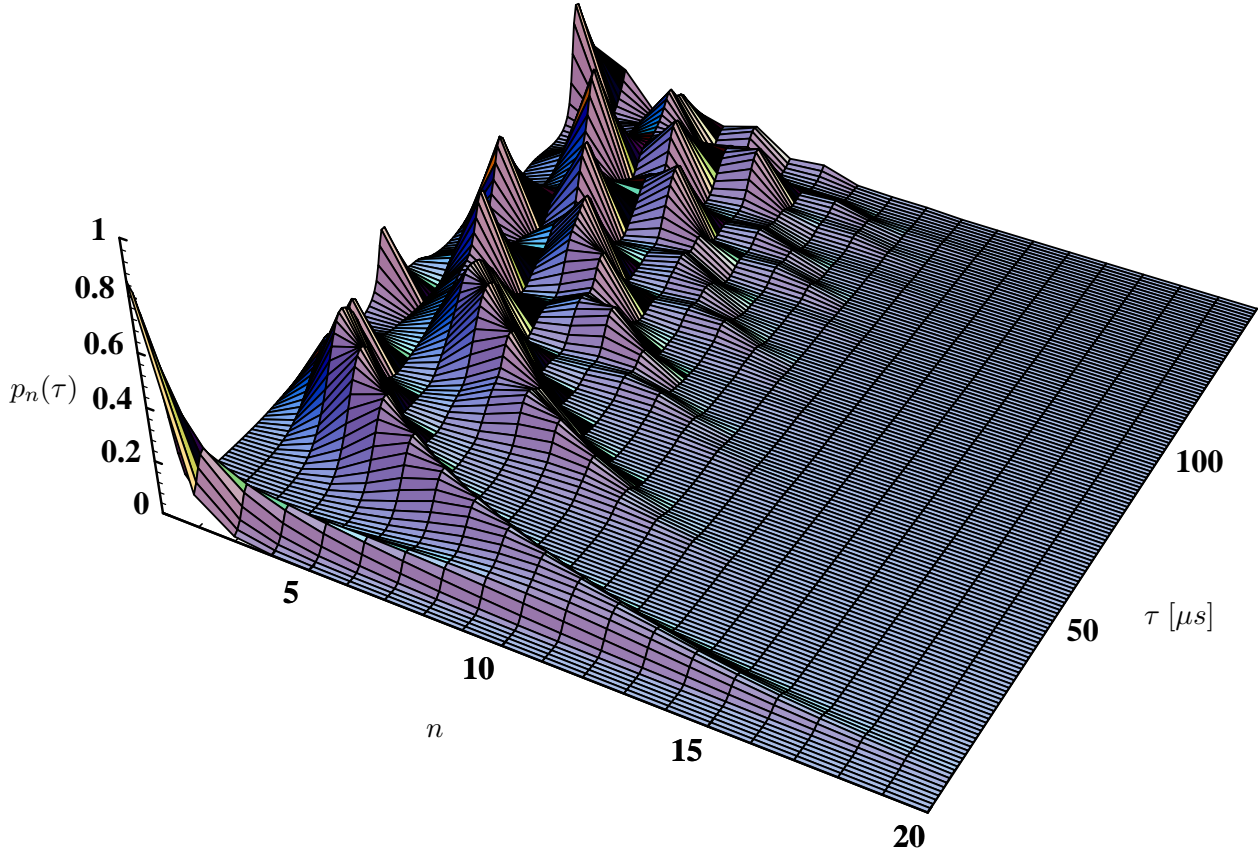


**Figure 1:** The rugged landscape of the photon distribution  $p_n(\tau)$  in Eq. (2.23) at equilibrium for the micromaser as a function of the number of photons in the cavity,  $n$ , and the atomic time-of-flight  $\tau$ . The parameters correspond to a superconducting niobium maser, cooled down to a temperature of  $T = 0.5$  K, with an average thermal photon occupation number of  $n_b = 0.15$ , at the maser frequency of 21.5 GHz. The single-photon Rabi frequency  $\Omega$  is 44 kHz, the photon lifetime in the cavity is  $T_{\text{cav}} = 0.2$  s, and the atomic beam intensity is  $R = 50$ /s.

## 2 Basic micromaser theory

In the micromaser a beam of excited atoms is sent through a cavity and each atom interacts with the cavity during a well-defined transit time  $\tau$ . The theory of the micromaser has been developed in [27, 28], and in this section we briefly review the standard theory, generally following the notation of that paper. We assume that excited atoms are injected into the cavity at an average rate  $R$  and that the typical decay rate for photons in the cavity is  $\gamma$ . The number of atoms passing the cavity in a single decay time  $N = R/\gamma$  is an important dimensionless parameter, effectively controlling the average number of photons stored in a high-quality cavity. We shall assume that the time  $\tau$  during which the atom interacts with the cavity is so small that effectively only one atom is found in the cavity at any time, i.e.  $R\tau \ll 1$ . A further simplification is introduced by assuming that the cavity decay time  $1/\gamma$  is much longer than the interaction time, i.e.  $\gamma\tau \ll 1$ , so that damping effects may be ignored while the atom passes through the cavity. This

point is further elucidated in Appendix A. In the typical experiment of Ref. [31] these quantities are given the values  $N = 10$ ,  $R\tau = 0.0025$  and  $\gamma\tau = 0.00025$ .

## 2.1 The Jaynes–Cummings Model

The electromagnetic interaction between a two-level atom with level separation  $\omega_0$  and a single mode with frequency  $\omega$  of the radiation field in a cavity is described, in the rotating wave approximation, by the Jaynes–Cummings (JC) Hamiltonian [14]

$$H = \omega a^* a + \frac{1}{2}\omega_0 \sigma_z + g(a\sigma_+ + a^*\sigma_-) , \quad (2.1)$$

where the coupling constant  $g$  is proportional to the dipole matrix element of the atomic transition<sup>1</sup>. We use the Pauli matrices to describe the two-level atom and the notation  $\sigma_{\pm} = (\sigma_x \pm i\sigma_y)/2$ . For  $g = 0$  the atom-plus-field states  $|n, s\rangle$  are characterized by the quantum number  $n = 0, 1, \dots$  of the oscillator and  $s = \pm$  for the atomic levels (with  $-$  denoting the ground state). At resonance  $\omega = \omega_0$  the levels  $|n-1, +\rangle$  and  $|n, -\rangle$  are degenerate for  $n \geq 1$  (excepting the ground state  $n = 0$ ), but this degeneracy is lifted by the interaction. For arbitrary coupling  $g$  and detuning parameter  $\Delta\omega = \omega_0 - \omega$  the system reduces to a  $2 \times 2$  eigenvalue problem, which may be trivially solved. The result is that two new levels are formed as superpositions of the previously degenerate ones with a separation in energy  $E_{n-1,+} - E_{n,-} = \sqrt{\Delta\omega^2 + 4g^2n}$ . The system performs Rabi oscillations with this frequency between the original, unperturbed states with transition probabilities [14]

$$\begin{aligned} |\langle n, - | e^{-iH\tau} | n, - \rangle|^2 &= 1 - q_n(\tau) , \\ |\langle n-1, + | e^{-iH\tau} | n, - \rangle|^2 &= q_n(\tau) , \\ |\langle n, + | e^{-iH\tau} | n, + \rangle|^2 &= 1 - q_{n+1}(\tau) , \\ |\langle n+1, - | e^{-iH\tau} | n, + \rangle|^2 &= q_{n+1}(\tau) . \end{aligned} \quad (2.2)$$

These are all expressed in terms of

$$q_n(\tau) = \frac{g^2 n}{g^2 n + \frac{1}{4}\Delta\omega^2} \sin^2 \left( \tau \sqrt{g^2 n + \frac{1}{4}\Delta\omega^2} \right) . \quad (2.3)$$

---

<sup>1</sup>This coupling constant turns out to be identical to the single photon Rabi frequency for the case of vanishing detuning, i.e.  $g = \Omega$ . There is actually some confusion in the literature about what is called the Rabi frequency [33]. With our definition, the energy separation between the shifted states at resonance is  $2\Omega$ .

Notice that for  $\Delta\omega = 0$  we have  $q_n = \sin^2(g\tau\sqrt{n})$ . Most of the following discussion will be limited to this case.

Denoting the probability of finding  $n$  photons in the cavity by  $p_n$  we find the conditional probability that an excited atom decays to the ground state in the cavity to be

$$\mathcal{P}(-) = \langle q_{n+1} \rangle = \sum_{n=0}^{\infty} q_{n+1} p_n . \quad (2.4)$$

It is this sum over the incommensurable frequencies  $g\sqrt{n}$  that is the cause of some of the most important properties of the micromaser, such as quantum collapse and revivals (see e.g. Refs. [34]–[36]). These effects are most easily displayed in the case that the cavity field is coherent with Poisson distribution

$$p_n = \frac{\langle n \rangle^n}{n!} e^{-\langle n \rangle} . \quad (2.5)$$

In the more realistic case, where the changes of the cavity field due to the passing atoms is taken into account, a complicated statistical state of the cavity arises [27], [37]–[39] (see Fig. 1). It is the details of this state that are investigated in this paper.

## 2.2 Mixed states

The above formalism is directly applicable when the atom and the radiation field are both in pure states initially. In general the statistical state of the system is described by an initial density matrix  $\rho$ , which evolves according to the usual rule  $\rho \rightarrow \rho(t) = \exp(-iHt)\rho\exp(iHt)$ . If we disregard, for the moment, the decay of the cavity field due to interactions with the environment, the evolution is governed by the JC Hamiltonian in Eq. (2.1). It is natural to assume that the atom and the radiation field of the cavity initially are completely uncorrelated so that the initial density matrix factorizes in a cavity part and a product of  $k$  atoms as

$$\rho = \rho_C \otimes \rho_{A_1} \otimes \rho_{A_2} \otimes \cdots \otimes \rho_{A_k} . \quad (2.6)$$

When the first atom  $A_1$  has passed through the cavity, part of this factorizability is destroyed by the interaction and the state has become

$$\rho(\tau) = \rho_{C,A_1}(\tau) \otimes \rho_{A_2} \otimes \cdots \otimes \rho_{A_k} . \quad (2.7)$$

The explicit form of the cavity-plus-atom entangled state  $\rho_{C,A_1}(\tau)$  is analysed in Appendix A. After the interaction, the cavity decays, more atoms pass through and the state becomes more and more entangled. If we decide never to measure

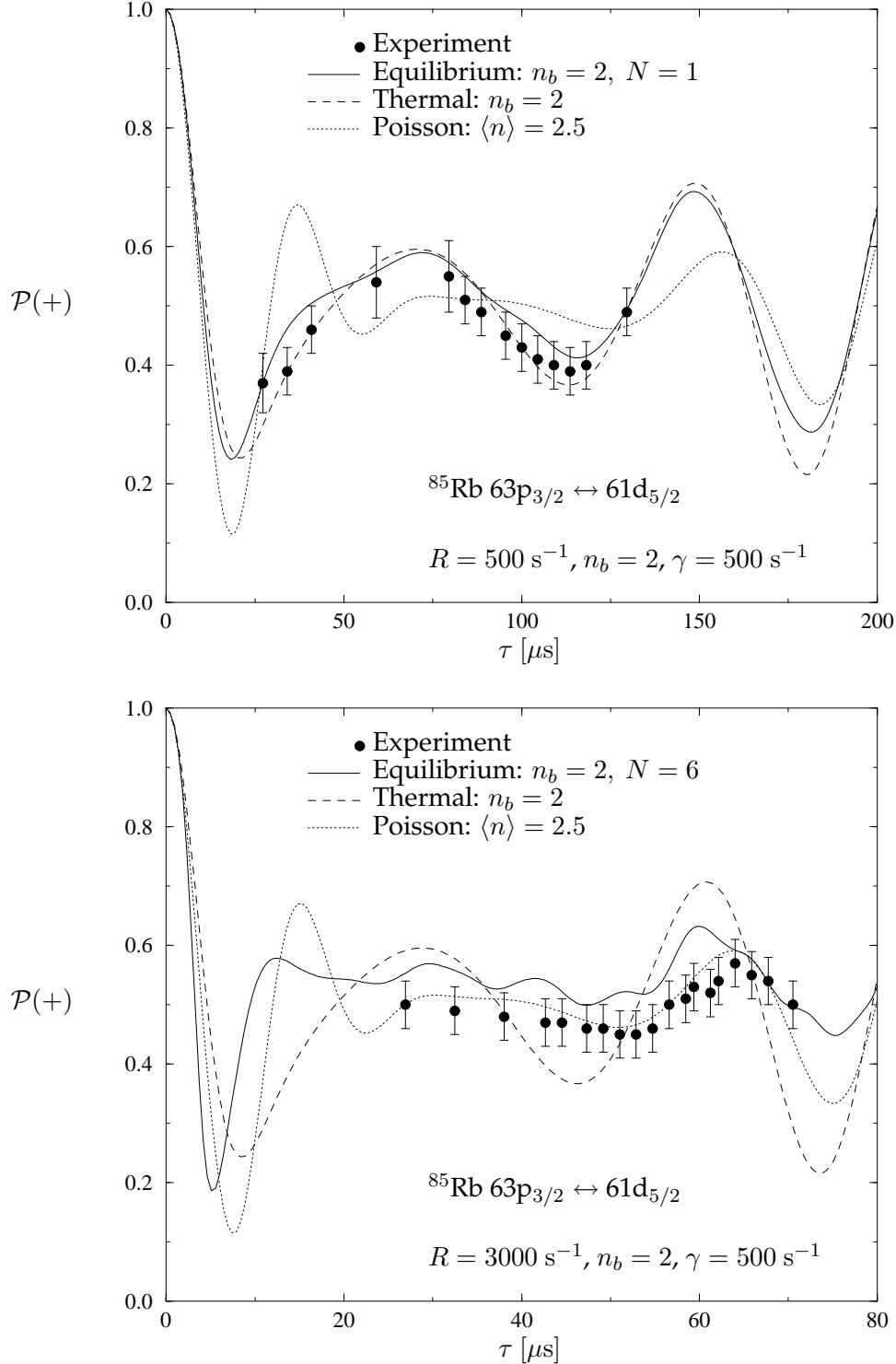


**Figure 2:** Comparison of  $\mathcal{P}(+) = 1 - \mathcal{P}(-) = 1 - \langle q_{n+1} \rangle$  with experimental data of Ref. [21] for various probability distributions. The Poisson distribution is defined in Eq. (2.5), the thermal in Eq. (2.16), and the micromaser equilibrium distribution in Eq. (2.23). In the upper figure ( $N = R/\gamma = 1$ ) the thermal distribution agrees well with the data and in the lower ( $N = 6$ ) the Poisson distribution fits the data best. It is curious that the data systematically seem to deviate from the micromaser equilibrium distribution. In the lower figure we have also corrected the erroneous time scale in Fig. 5 of Ref. [21].

the state of atoms  $A_1 \dots A_i$  with  $i < k$ , we should calculate the trace over the corresponding states and only the  $\rho_0$ -component remains. Since the time evolution is linear, each of the components in Eq. (2.7) evolves independently, and it does not matter when we calculate the trace. We can do it after each atom has passed the cavity, or at the end of the experiment. For this we do not even have to assume that the atoms are non-interacting after they leave the cavity, even though this simplifies the time evolution. If we do perform a measurement of the state of an intermediate atom  $A_i$ , a correlation can be observed between that result and a measurement of atom  $A_k$ , but the statistics of the unconditional measurement of  $A_k$  is not affected by a measurement of  $A_i$ . In a real experiment also the efficiency of the measuring apparatus should be taken into account when using the measured results from atoms  $A_1, \dots, A_i$  to predict the probability of the outcome of a measurement of  $A_k$  (see Ref. [32] for a detailed investigation of this case).

As a generic case let us assume that the initial state of the atom is a diagonal mixture of excited and unexcited states

$$\rho_A = \begin{pmatrix} a & 0 \\ 0 & b \end{pmatrix} , \quad (2.8)$$

where, of course,  $a, b \geq 0$  and  $a + b = 1$ . Using that both preparation and observation are diagonal in the atomic states, it may now be seen from the transition elements in Eq. (2.2) that the time evolution of the cavity density matrix does not mix different diagonals of this matrix. Each diagonal so to speak “lives its own life” with respect to dynamics. This implies that if the initial cavity density matrix is diagonal, i.e. of the form

$$\rho_C = \sum_{n=0}^{\infty} p_n |n\rangle \langle n| , \quad (2.9)$$

with  $p_n \geq 0$  and  $\sum_{n=0}^{\infty} p_n = 1$ , then it stays diagonal during the interaction between atom and cavity and may always be described by a probability distribution  $p_n(t)$ . In fact, we easily find that after the interaction we have

$$p_n(\tau) = aq_n(\tau)p_{n-1} + bq_{n+1}(\tau)p_{n+1} + (1 - aq_{n+1}(\tau) - bq_n(\tau))p_n , \quad (2.10)$$

where the first term is the probability of decay for the excited atomic state, the second the probability of excitation for the atomic ground state, and the third is the probability that the atom is left unchanged by the interaction. It is convenient to write this in matrix form

$$p(\tau) = M(\tau)p , \quad (2.11)$$

with a transition matrix  $M = M(+) + M(-)$  composed of two parts, representing that the outgoing atom is either in the excited state (+) or in the ground state (-). Explicitly we have

$$\begin{aligned} M(+)_{nm} &= b q_{n+1} \delta_{n+1,m} + a(1 - q_{n+1}) \delta_{n,m} , \\ M(-)_{nm} &= a q_n \delta_{n,m+1} + b(1 - q_n) \delta_{n,m} . \end{aligned} \quad (2.12)$$

Notice that these formulas are completely classical and may be simulated with a standard Markov process. The statistical properties are not quantum mechanical as long as the incoming atoms have a diagonal density matrix and we only measure elements in the diagonal. The only quantum mechanical feature at this stage is the discreteness of the photon states, which has important consequences for the correlation length (see Section 2.3). If the atomic density matrix has off-diagonal elements, the above formalism breaks down. The reduced cavity density matrix will then also develop off-diagonal elements, even if initially it is diagonal. We shall not go further into this question here (see for example Refs. [40]–[42]).

### 2.3 The lossless cavity

The above discrete master equation (2.10) describes the pumping of a lossless cavity with a beam of atoms. After  $k$  atoms have passed through the cavity, its state has become  $M^k p$ . In order to see whether this process may reach statistical equilibrium for  $k \rightarrow \infty$  we write Eq. (2.10) in the form

$$p_n(\tau) = p_n + J_{n+1} - J_n , \quad (2.13)$$

where  $J_n = -a q_n p_{n-1} + b q_n p_n$ . In statistical equilibrium we must have  $J_{n+1} = J_n$ , and the common value  $J = J_n$  for all  $n$  can only be zero since  $p_n$ , and therefore  $J$ , has to vanish for  $n \rightarrow \infty$ . It follows that this can only be the case for  $a < b$  i.e.  $a < 0.5$ . There must thus be fewer than 50% excited atoms in the beam, otherwise the lossless cavity blows up. If  $a < 0.5$ , the cavity will reach an equilibrium distribution of the form of a thermal distribution for an oscillator  $p_n = (1 - a/b)(a/b)^n$ . The statistical equilibrium may be shown to be stable, i.e. that all non-trivial eigenvalues of the matrix  $M$  are real and smaller than 1.

### 2.4 The dissipative cavity

A single oscillator interacting with an environment having a huge number of degrees of freedom, for example a heat bath, dissipates energy according to the well-known damping formula (see for example [44, 45]):

$$\begin{aligned}
\frac{d\rho_C}{dt} = & i[\rho_C, \omega a^* a] \\
& -\frac{1}{2}\gamma(n_b + 1)(a^* \rho_C + \rho_C a^* a - 2a \rho_C a^*) \\
& -\frac{1}{2}\gamma n_b(a a^* \rho_C + \rho_C a a^* - 2a^* \rho_C a) ,
\end{aligned} \tag{2.14}$$

where  $n_b$  is the average environment occupation number at the oscillator frequency and  $\gamma$  is the decay constant. This evolution also conserves diagonality, so we have for any diagonal cavity state:

$$\frac{1}{\gamma} \frac{dp_n}{dt} = -(n_b + 1)(np_n - (n + 1)p_{n+1}) - n_b((n + 1)p_n - np_{n-1}) , \tag{2.15}$$

which of course conserves probability. The right-hand side may as for Eq. (2.13) be written as  $J_{n+1} - J_n$  with  $J_n = (n_b + 1)np_n - n_b np_{n-1}$  and the same arguments as above lead to a thermal equilibrium distribution with

$$p_n = \frac{1}{1 + n_b} \left( \frac{n_b}{1 + n_b} \right)^n . \tag{2.16}$$

## 2.5 The discrete master equation

We now take into account both pumping and damping. Let the next atom arrive in the cavity after a time  $T \gg \tau$ . During this interval the cavity damping is described by Eq. (2.15), which we shall write in the form

$$\frac{dp}{dt} = -\gamma L_C p , \tag{2.17}$$

where  $L_C$  is the cavity decay matrix from above

$$(L_C)_{nm} = (n_b + 1)(n\delta_{n,m} - (n + 1)\delta_{n+1,m}) + n_b((n + 1)\delta_{n,m} - n\delta_{n-1,m}) . \tag{2.18}$$

The statistical state of the cavity when the next atom arrives is thus given by

$$p(T) = e^{-\gamma L_C T} M(\tau) p . \tag{2.19}$$

In using the full interval  $T$  and not  $T - \tau$  we allow for the decay of the cavity in the interaction time, although this decay is not properly included with the atomic interaction (for a correct treatment see Appendix A).

This would be the master equation describing the evolution of the cavity if the atoms in the beam arrived with definite and known intervals. More commonly, the time intervals  $T$  between atoms are Poisson-distributed according to  $d\mathcal{P}(T) = \exp(-RT)RdT$  with an average time interval  $1/R$  between them. Averaging the exponential in Eq. (2.19) we get

$$\langle p(T) \rangle_T = Sp , \quad (2.20)$$

where

$$S = \frac{1}{1 + L_C/N} M , \quad (2.21)$$

and  $N = R/\gamma$  is the dimensionless pumping rate already introduced.

Implicit in the above consideration is the lack of knowledge of the actual value of the atomic state after the interaction. If we know that the state of the atom is  $s = \pm$  after the interaction, then the average operator that transforms the cavity state is instead

$$S(s) = (1 + L_C/N)^{-1} M(s) , \quad (2.22)$$

with  $M(s)$  given by Eq. (2.12).

Repeating the process for a sequence of  $k$  unobserved atoms we find that the initial probability distribution  $p$  becomes  $S^k p$ . In the general case this Markov process converges towards a statistical equilibrium state satisfying  $Sp = p$ , which has the solution [27, 41] for  $n \geq 1$

$$p_n = p_0 \prod_{m=1}^n \frac{n_b m + N a q_m}{(1 + n_b) m + N b q_m} . \quad (2.23)$$

The overall constant  $p_0$  is determined by  $\sum_{n=0}^{\infty} p_n = 1$ . The photon landscape formed by this expression as a function of  $n$  and  $\tau$  is shown in Fig. 1 for  $a = 1$  and  $b = 0$ . For greater values of  $\tau$  it becomes very rugged.

### 3 Correlations

After studying stationary single-time properties of the micromaser, such as the average photon number in the cavity and the average excitation of the outgoing atoms, we now proceed to dynamical properties. Correlations between outgoing atoms are not only determined by the equilibrium distribution in the cavity but also by its approach to this equilibrium. Short-time correlations are difficult to determine experimentally, because they require efficient observation of the states

of atoms emerging from the cavity in rapid succession. We propose instead to study and measure long-time correlations, which do not impose the same strict experimental conditions. These correlations turn out to have a surprisingly rich structure (see Fig. 5) and reflect global properties of the photon distribution. In this section we introduce the concept of long-time correlations and present two ways of calculating them numerically. In the following sections we study the analytic properties of these correlations and elucidate their relation to the dynamical phase structure, especially those aspects that are poorly seen in the single-time observables or short-time correlations.

### 3.1 Atomic beam observables

Let us imagine that we know the state of all the atoms as they enter the cavity, for example that they are all excited, and that we are able to determine the state of each atom as it exits from the cavity. We shall assume that the initial beam is statistically stationary, described by the density matrix (2.8), and that we have obtained an experimental record of the exit states of all the atoms after the cavity has reached statistical equilibrium with the beam. From this record we may estimate a number of quantities, for example the probability of finding the atom in a state  $s = \pm$  after the interaction, where we choose  $+$  to represent the excited state and  $-$  the ground state. The probability may be expressed in the matrix form

$$\mathcal{P}(s) = u^0{}^\top M(s)p^0 , \quad (3.1)$$

where  $M(s)$  is given by Eq. (2.12) and  $p^0$  is the equilibrium distribution (2.23). The quantity  $u^0$  is a vector with all entries equal to 1,  $u_n^0 = 1$ , and represents the sum over all possible final states of the cavity. In Fig. 2 we have compared the behaviour of  $\mathcal{P}(+)$  with some characteristic experiments.

Since  $\mathcal{P}(+) + \mathcal{P}(-) = 1$  it is sufficient to measure the average spin value (see Fig. 3):

$$\langle s \rangle = \mathcal{P}(+) - \mathcal{P}(-) . \quad (3.2)$$

Since  $s^2 = 1$  this quantity also determines the variance to be  $\langle s^2 \rangle - \langle s \rangle^2 = 1 - \langle s \rangle^2$ .

Correspondingly, we may define the joint probability for observing the states of two atoms,  $s_1$  followed  $s_2$ , with  $k$  unobserved atoms between them,

$$\mathcal{P}_k(s_1, s_2) = u^0{}^\top S(s_2)S^kS(s_1)p^0 , \quad (3.3)$$

where  $S$  and  $S(s)$  are defined in Eqs. (2.21) and (2.22). It is worth noticing that since  $S = S(+) + S(-)$  and  $Sp^0 = p^0$  we have  $\sum_{s_1} \mathcal{P}_k(s_1, s_2) = \mathcal{P}(s_2)$ . Since we also have  $u^0{}^\top L = u^0{}^\top (M - 1) = 0$  we find likewise that  $u^0{}^\top S = u^0{}^\top$  so that

$\sum_{s_2} \mathcal{P}_k(s_1, s_2) = \mathcal{P}(s_1)$ . Combining these relations we derive that  $\mathcal{P}_k(+, -) = \mathcal{P}_k(-, +)$ , as expected. Due to these relations there is essentially only one two-point function, namely the “spin–spin” covariance function

$$\begin{aligned} \langle ss \rangle_k &= \sum_{s_1, s_2} s_1 s_2 \mathcal{P}_k(s_1, s_2) \\ &= \mathcal{P}_k(+, +) + \mathcal{P}_k(-, -) - \mathcal{P}_k(+, -) - \mathcal{P}_k(-, +) \\ &= 1 - 4\mathcal{P}_k(+, -) . \end{aligned} \quad (3.4)$$

From this we derive the properly normalized correlation function

$$\gamma_k^A = \frac{\langle ss \rangle_k - \langle s \rangle^2}{1 - \langle s \rangle^2} , \quad (3.5)$$

which satisfies  $-1 \leq \gamma_k^A \leq 1$ .

At large times, when  $k \rightarrow \infty$ , the correlation function is in general expected to decay exponentially, and we define the atomic beam correlation length  $\xi_A$  by the asymptotic behaviour for large  $k \simeq Rt$

$$\gamma_k^A \sim \exp\left(-\frac{k}{R\xi_A}\right) . \quad (3.6)$$

Here we have scaled with  $R$ , the average number of atoms passing the cavity per unit of time, so that  $\xi_A$  is the typical length of time that the cavity remembers previous pumping events.

### 3.2 Cavity observables

In the context of the micromaser cavity, one relevant observable is the instantaneous number of photons  $n$ , from which we may form the average  $\langle n \rangle$  and correlations in time. The quantum state of light in the cavity is often characterized by the Fano–Mandel quality factor [48], which is related to the fluctuations of  $n$  through

$$Q_f = \frac{\langle n^2 \rangle - \langle n \rangle^2}{\langle n \rangle} - 1 . \quad (3.7)$$

This quantity vanishes for coherent (Poisson) light and is positive for classical light (see Fig. 3).

In equilibrium there is a relation between the average photon occupation number and the spin average in the atomic beam, which is trivial to derive from the equilibrium distribution

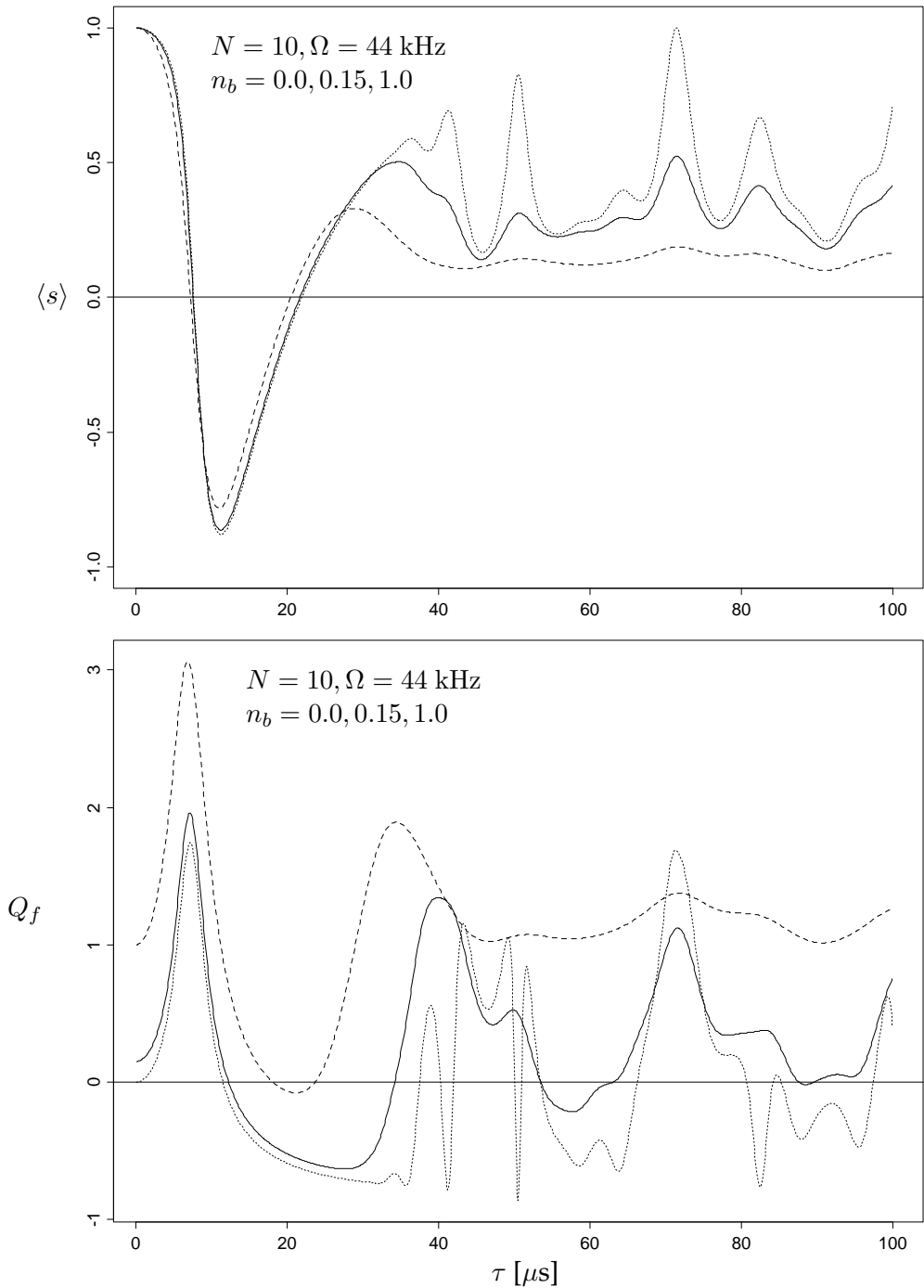


**Figure 3:** The upper figure shows the mean value of the spin variable as a function of the atomic passage time for three different values of  $n_b$ . The dotted line  $n_b = 0$ , the solid line  $n_b = 0.15$ , and the dashed line  $n_b = 1$ . The lower figure shows the Mandel quality factor in the same region for the same values of  $n_b$ . The pronounced structures in the case of  $n_b = 0$  are caused by trapping states (see Section 7.1).

$$\langle n \rangle = u^0 \hat{n} p^0 = n_b + N \mathcal{P}(-) = n_b + N \frac{1 - \langle s \rangle}{2} , \quad (3.8)$$

where  $\hat{n}$  is a diagonal matrix representing the quantum number  $n$ . A similar but more uncertain relation between the Mandel quality factor and fluctuations in the atomic beam may also be derived [29].

The covariance between the values of the photon occupation number  $k$  atoms apart in equilibrium is easily seen to be given by

$$\langle nn \rangle_k = u^0 \hat{n} S^k \hat{n} p^0 , \quad (3.9)$$

and again a normalized correlation function may be defined

$$\gamma_k^C = \frac{\langle nn \rangle_k - \langle n \rangle^2}{\langle n^2 \rangle - \langle n \rangle^2} . \quad (3.10)$$

The cavity correlation length  $\xi_C$  is defined by

$$\gamma_k^C \sim \exp \left( -\frac{k}{R \xi_C} \right) . \quad (3.11)$$

Since the same power of the matrix  $S$  is involved, both correlation lengths are determined by the same eigenvalue, and the two correlation lengths are therefore identical  $\xi_A = \xi_C = \xi$  and we shall no longer distinguish between them.

### 3.3 Monte Carlo determination of correlation lengths

Since the statistical behaviour of the micromaser is a classical Markov process it is possible to simulate it by means of Monte Carlo methods using the cavity occupation number  $n$  as stochastic variable.

A sequence of excited atoms is generated at Poisson-distributed times and are allowed to act on  $n$  according to the probabilities given by Eq. (2.2). In these simulations we have for simplicity chosen  $a = 1$  and  $b = 0$ . After the interaction the cavity is allowed to decay during the waiting time until the next atom arrives. The action of this process on the cavity variable  $n$  is simulated by means of the transition probabilities read off from the dissipative master equation (2.15) using a suitably small time step  $dt$ . The states of the atoms in the beam are determined by the pumping transitions and the atomic correlation function may be determined from this sequence of spin values by making suitable averages after the system has reached equilibrium. Finally the correlation lengths may be extracted numerically from the Monte Carlo data.

This extraction is, however, limited by noise due to the finite sample size which in our simulation is  $10^6$  atoms. In regions where the correlation length

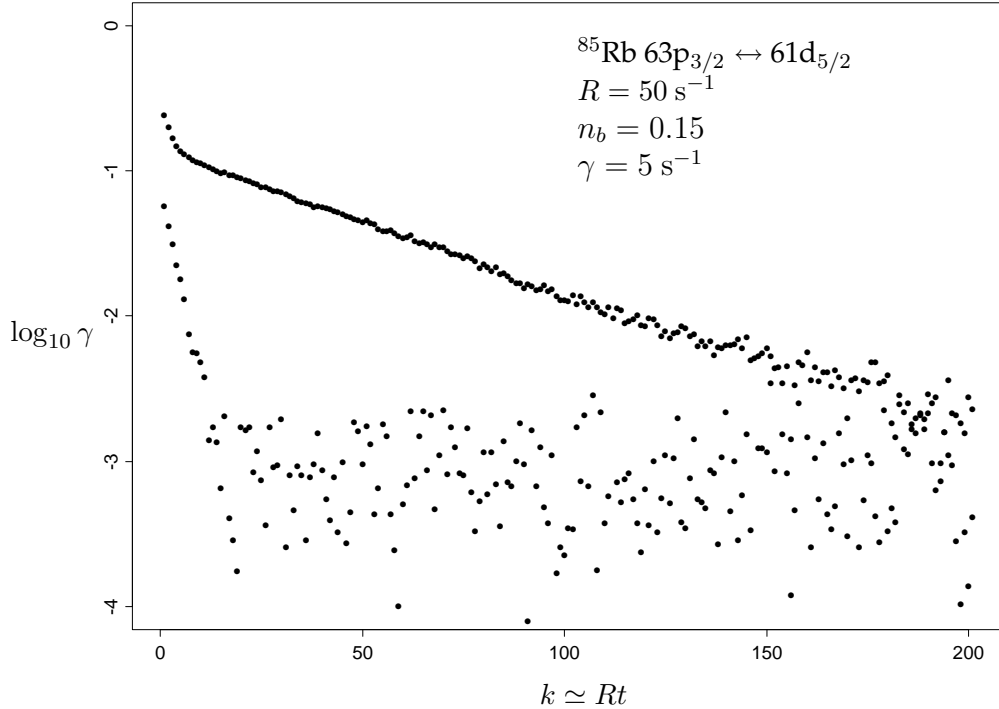


**Figure 4:** Monte Carlo data (with  $10^6$  simulated atoms) for the correlation as a function of the separation  $k \simeq Rt$  between the atoms in the beam for  $\tau = 25 \mu\text{s}$  (lower data points) and  $\tau = 50 \mu\text{s}$  (upper data points). In the latter case the exponential decay at large times is clearly visible, whereas it is hidden in the noise in the former. The parameters are those of the experiment described in Ref. [31].

is large, it is fairly easy to extract it by fitting to the exponential decay, whereas it is more difficult in the regions where it is small (see Fig. 4). This accounts for the differences between the exact numerical calculations and the Monte Carlo data in Fig. 5. It is expected that real experiments will face the same type of problems in extracting the correlation lengths from real data.

### 3.4 Numerical calculation of correlation lengths

The micromaser equilibrium distribution is the solution of  $Sp = p$ , where  $S$  is the one-atom propagation matrix (2.21), so that  $p^0$  is an eigenvector of  $S$  from the right with eigenvalue  $\kappa_0 = 1$ . The corresponding eigenvector from the left is  $u^0$  and normalization of probabilities is expressed as  $u^{0\top} p^0 = 1$ . The general eigenvalue problem concerns solutions to  $Sp = \kappa p$  from the right and  $u^\top S = \kappa u^\top$  from the left. It is shown below that the eigenvalues are non-degenerate, which implies that there exists a spectral resolution of the form

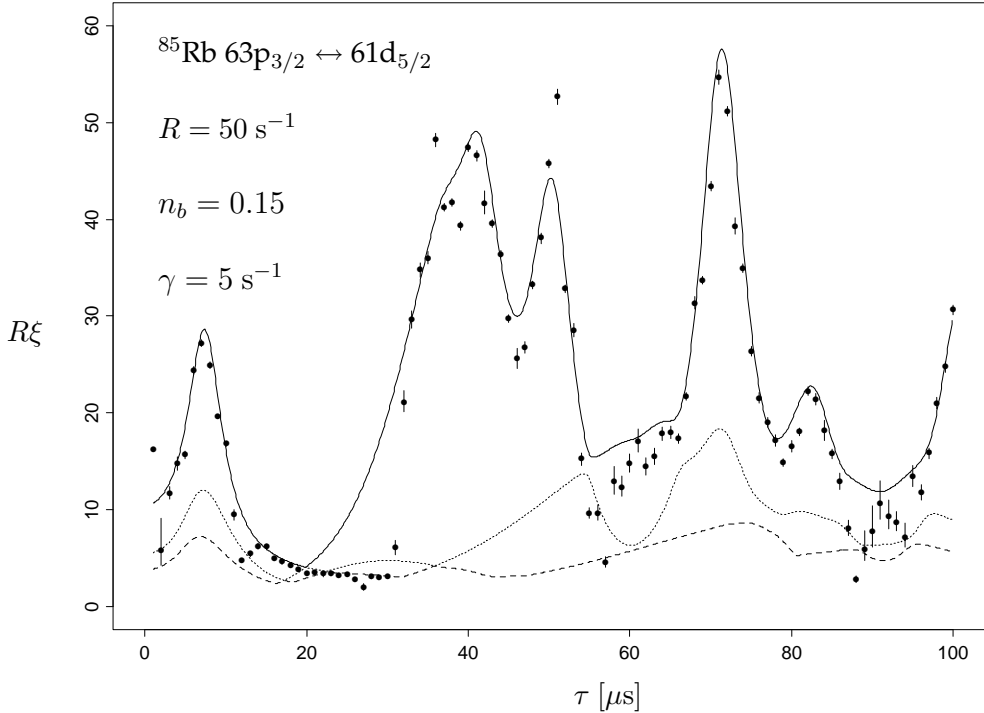


**Figure 5:** Comparison of theory (solid curve) and MC data (dots) for the correlation length  $R\xi$  (sample size  $10^6$  atoms). The dotted and dashed curves correspond to sub-leading eigenvalues ( $\kappa_{2,3}$ ) of the matrix  $S$ . The parameters are those of the experiment in Ref. [31].

$$S = \sum_{\ell=0}^{\infty} \kappa_{\ell} p^{\ell} u^{\ell \top} , \quad (3.12)$$

with eigenvalues  $\kappa_{\ell}$  and eigenvectors  $p^{\ell}$  and  $u^{\ell}$  from right and left respectively. The long-time behaviour of the correlation function is governed by the next-to-leading eigenvalue  $\kappa_1 < 1$ , and we see that

$$R\xi = -\frac{1}{\log \kappa_1} . \quad (3.13)$$

The eigenvalues are determined by the characteristic equation  $\det\{S - \kappa\} = 0$ , which may be solved numerically. This procedure is, however, not well-defined for the infinite-dimensional matrix  $S$ , and in order to evaluate the determinant we have truncated the matrix to a large and finite-size  $K \times K$  with typical  $K \simeq 100$ . The explicit form of  $S$  in Eq. (2.21) is used, which reduces the problem to the calculation of the determinant for a Jacobi matrix. Such a matrix vanishes outside the main diagonal and the two subleading diagonals on each side. It is shown in Section 4.3 that the eigenvalues found from this equation are indeed

non-degenerate, real, positive and less than unity.

The next-to-leading eigenvalue is shown in Fig. 5 and agrees very well with the Monte Carlo calculations. This figure shows a surprising amount of structure and part of the effort in the following will be to understand this structure in detail.

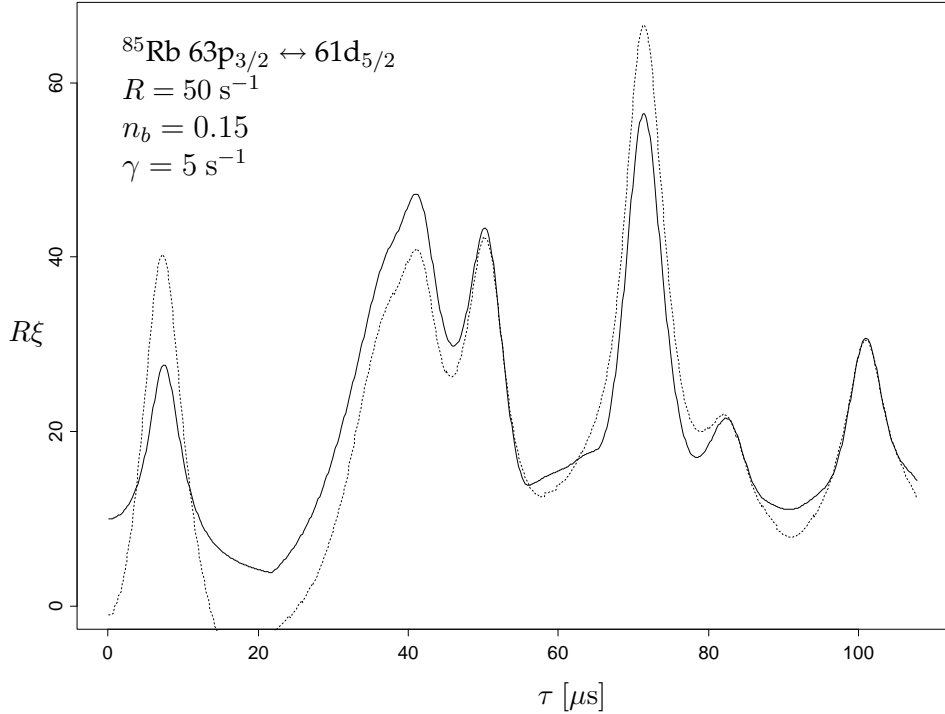


**Figure 6:** Comparison of the sum in Eq. (3.14) over reciprocal eigenvalues (dotted curve) with numerically determined correlation length (solid curve) for the same parameters as in Fig. 5. The difference between the curves is entirely due to the subdominant eigenvalues that have not been taken into account here.

It is possible to derive an exact sum rule for the reciprocal eigenvalues (see Appendix B), which yields the approximate expression:

$$\xi \simeq 1 + \sum_{n=1}^{\infty} \left( \frac{P_n(1 - P_n)}{(1 + n_b)np_n} - \frac{1 - [n_b/(1 + n_b)]^n}{n} \right) , \quad (3.14)$$

when the subdominant eigenvalues may be ignored. Here  $p_n$  is the equilibrium distribution Eq. (2.23) and  $P_n = \sum_{m=0}^{n-1} p_m$  is the cumulative probability. In Fig. 6 we compare the exact numerical calculation and the result of the sum rule, which is much less time-consuming to compute.

## 4 Analytic preliminaries

In order to tackle the task of determining the phase structure in the micromaser we need to develop some mathematical tools. The dynamics can be formulated in two different ways which are equivalent in the large flux limit. Both are related to Jacobi matrices describing the stochastic process. Many characteristic features of the correlation length are related to scaling properties for  $N \rightarrow \infty$ , and require a detailed analysis of the continuum limit. Here we introduce some of the concepts that are used in the main analysis in Section 5.

### 4.1 Continuous master equation

When the atoms have Poisson distributed arrival times it is possible to formulate the problem as a differential equation [41]. Each atom has the same probability  $Rdt$  of arriving in an infinitesimal time interval  $dt$ . Provided the interaction with the cavity takes less time than this interval, i.e.  $\tau \ll dt$ , we may consider the transition to be instantaneous and write the transition matrix as  $Rdt(M - 1)$  so that we get

$$\frac{dp}{dt} = -\gamma L_C p + R(M - 1)p \equiv -\gamma L p , \quad (4.1)$$

where  $L = L_C - N(M - 1)$ . This equation obviously has the solution

$$p(t) = e^{-\gamma Lt} p . \quad (4.2)$$

Explicitly we have

$$\begin{aligned} L_{nm} &= (n_b + 1)(n\delta_{n,m} - (n + 1)\delta_{n+1,m}) + n_b((n + 1)\delta_{n,m} - n\delta_{n,m+1}) \\ &\quad + N((aq_{n+1} + bq_n)\delta_{n,m} - aq_n\delta_{n,m+1} - bq_{n+1}\delta_{n+1,m}) , \end{aligned} \quad (4.3)$$

and

$$\begin{aligned} \frac{1}{\gamma} \frac{dp_n}{dt} &= -(n_b + 1)(np_n - (n + 1)p_{n+1}) - n_b((n + 1)p_n - np_{n-1}) \\ &\quad - N((aq_{n+1} + bq_n)p_n - aq_n p_{n-1} - bq_{n+1} p_{n+1}) . \end{aligned} \quad (4.4)$$

The equilibrium distribution may be found by the same technique as before, writing the right-hand side of Eq. (4.4) as  $J_{n+1} - J_n$  with

$$J_n = ((n_b + 1)n + Nbq_n)p_n - (n_b n + Naq_n)p_{n-1} , \quad (4.5)$$

and setting  $J_n = 0$  for all  $n$ . The equilibrium distribution is clearly given by the same expression (2.23) as in the discrete case.

## 4.2 Relation to the discrete case

Even if the discrete and continuous formulation has the same equilibrium distribution, there is a difference in the dynamical behaviour of the two cases. In the discrete case the basic propagation matrix is  $S^k$ , where  $S = (1 + L_C/N)^{-1}M$ , whereas it is  $\exp(-\gamma Lt)$  in the continuous case. For high pumping rate  $N$  we expect the two formalisms to coincide, when we identify  $k \simeq Rt$ . For the long-time behaviour of the correlation functions this implies that the next-to-leading eigenvalues  $\kappa_1$  of  $S$  and  $\lambda_1$  of  $L$  must be related by  $1/\xi = \gamma\lambda_1 \simeq -R \log \kappa_1$ .

To prove this, let us compare the two eigenvalue problems. For the continuous case we have

$$(L_C - N(M - 1))p = \lambda p , \quad (4.6)$$

whereas in the discrete case we may rewrite  $Sp = \kappa p$  to become

$$\left( L_C - \frac{N}{\kappa}(M - 1) \right) p = N \left( \frac{1}{\kappa} - 1 \right) p . \quad (4.7)$$

Let a solution to the continuous case be  $p(N)$  with eigenvalue  $\lambda(N)$ , making explicit the dependence on  $N$ . It is then obvious that  $p(N/\kappa)$  is a solution to the discrete case with eigenvalue  $\kappa$  determined by

$$\lambda \left( \frac{N}{\kappa} \right) = N \left( \frac{1}{\kappa} - 1 \right) . \quad (4.8)$$

As we shall see below, for  $N \gg 1$  the next-to-leading eigenvalue  $\lambda_1$  stays finite or goes to zero, and hence  $\kappa_1 \rightarrow 1$  at least as fast as  $1/N$ . Using this result it follows that the correlation length is the same to  $\mathcal{O}(1/N)$  in the two formalisms.

## 4.3 The eigenvalue problem

The transition matrix  $L$  truncated to size  $(K + 1) \times (K + 1)$  is a special kind of asymmetric Jacobi matrix

$$L_K = \begin{pmatrix} A_0 + B_0 & -B_1 & 0 & 0 & \cdots \\ -A_0 & A_1 + B_1 & -B_2 & 0 & \cdots \\ 0 & -A_1 & A_2 + B_2 & -B_3 & \\ \vdots & \vdots & \vdots & \vdots & \vdots \\ & & & -A_{K-2} & A_{K-1} + B_{K-1} & -B_K \\ & & & \cdots & 0 & -A_{K-1} & A_K + B_K \end{pmatrix}, \quad (4.9)$$

where

$$\begin{aligned} A_n &= n_b(n+1) + N a q_{n+1} , \\ B_n &= (n_b + 1)n + N b q_n . \end{aligned} \quad (4.10)$$

Notice that the sum over the elements in every column vanishes, except for the first and the last, for which the sums respectively take the values  $B_0$  and  $A_K$ . In our case we have  $B_0 = 0$ , but  $A_K$  is non-zero. For  $B_0 = 0$  it is easy to see (using row manipulation) that the determinant becomes  $A_0 A_1 \cdots A_K$  and obviously diverges in the limit of  $K \rightarrow \infty$ . Hence the truncation is absolutely necessary. All the coefficients in the characteristic equation diverge, if we do not truncate. In order to secure that there is an eigenvalue  $\lambda = 0$ , we shall force  $A_K = 0$  instead of the value given above. This means that the matrix is not just truncated but actually changed in the last diagonal element. Physically this secures that there is no external input to the process from cavity occupation numbers above  $K$ , a not unreasonable requirement.

An eigenvector to the right satisfies the equation  $L_K p = \lambda p$ , which takes the explicit form

$$-A_{n-1}p_{n-1} + (A_n + B_n)p_n - B_{n+1}p_{n+1} = \lambda p_n . \quad (4.11)$$

Since we may solve this equation successively for  $p_1, p_2, \dots, p_K$  given  $p_0$ , it follows that all eigenvectors are non-degenerate. The characteristic polynomial obeys the recursive equation

$$\det(L_K - \lambda) = (A_K + B_K - \lambda) \det(L_{K-1} - \lambda) - A_{K-1}B_K \det(L_{K-2} - \lambda) , \quad (4.12)$$

and this is also the characteristic equation for a symmetric Jacobi matrix with off-diagonal elements  $C_n = -\sqrt{A_{n-1}B_n}$ . Hence the eigenvalues are the same and therefore all real and, as we shall see below, non-negative. They may therefore be

ordered  $0 = \lambda_0 < \lambda_1 < \dots < \lambda_K$ . The equilibrium distribution (2.23) corresponds to  $\lambda = 0$  and is given by

$$p_n^0 = p_0^0 \prod_{m=1}^n \frac{A_{m-1}}{B_m} = p_0^0 \frac{A_0 A_1 \cdots A_{n-1}}{B_1 B_2 \cdots B_n} \quad \text{for } n = 1, 2, \dots, K . \quad (4.13)$$

Notice that this expression does not involve the vanishing values  $B_0 = A_K = 0$ .

Corresponding to each eigenvector  $p$  to the right there is an eigenvector  $u$  to the left, satisfying  $u^\top L_K = \lambda u^\top$ , which in components reads

$$A_n(u_n - u_{n-1}) + B_n(u_n - u_{n+1}) = \lambda u_n . \quad (4.14)$$

For  $\lambda = 0$  we obviously have  $u_n^0 = 1$  for all  $n$  and the scalar product  $u^0 \cdot p^0 = 1$ . The eigenvector to the left is trivially related to the eigenvector to the right via the equilibrium distribution

$$p_n = p_n^0 u_n . \quad (4.15)$$

The full set of eigenvectors to the left and to the right  $\{u^\ell, p^\ell \mid \ell = 0, 1, 2, \dots, K\}$  may now be chosen to be orthonormal  $u^\ell \cdot p^{\ell'} = \delta_{\ell, \ell'}$ , and is, of course, complete since the dimension  $K$  is finite.

It is useful to express this formalism in terms of averages over the equilibrium distribution  $\langle f_n \rangle_0 = \sum_{n=0}^K f_n p_n^0$ . Then using Eq. (4.15) we have, for an eigenvector with  $\lambda > 0$ , the relations

$$\begin{aligned} \langle u_n \rangle_0 &= 0 , \\ \langle u_n^2 \rangle_0 &= 1 , \\ \langle u_n u_n' \rangle_0 &= 0 \quad \text{for } \lambda \neq \lambda' . \end{aligned} \quad (4.16)$$

Thus the eigenvectors with  $\lambda > 0$  may be viewed as uncorrelated stochastic functions of  $n$  with zero mean and unit variance.

Finally, we rewrite the eigenvalue equation to the right in the form of  $\lambda p_n = J_n - J_{n+1}$  with

$$J_n = B_n p_n - A_{n-1} p_{n-1} = p_n^0 B_n (u_n - u_{n-1}) . \quad (4.17)$$

Using the orthogonality we then find

$$\lambda = \sum_{n=0}^K u_n (J_n - J_{n+1}) = \langle B_n (u_n - u_{n-1})^2 \rangle_0 , \quad (4.18)$$

which incidentally proves that all eigenvalues are non-negative. It is also evident that an eigenvalue is built up from the non-constant parts, i.e. the jumps of  $u_n$ .

#### 4.4 Effective potential

It is convenient to introduce an effective potential  $V_n$  by writing the equilibrium distribution (2.23) in the form

$$p_n = \frac{1}{Z} e^{-NV_n} , \quad (4.19)$$

with

$$V_n = -\frac{1}{N} \sum_{m=1}^n \log \frac{n_b m + N a q_m}{(1+n_b)m + N b q_m} , \quad (4.20)$$

for  $n \geq 1$ . The value of the potential for  $n = 0$  may be chosen arbitrarily, for example  $V_0 = 0$ , because of the normalization constant

$$Z = \sum_{n=0}^{\infty} e^{-NV_n} . \quad (4.21)$$

It is, of course, completely equivalent to discuss the shape of the equilibrium distribution and the shape of the effective potential.

#### 4.5 Semicontinuous formulation

Another way of making analytical methods, such as the Fokker–Planck equation, easier to use is to rewrite the formalism (exactly) in terms of the scaled photon number variable  $x$  and the scaled time parameter  $\theta$ , defined by

$$\begin{aligned} x &= \frac{n}{N} , \\ \theta &= g\tau\sqrt{N} . \end{aligned} \quad (4.22)$$

Notice that the variable  $x$  and not  $n$  is the natural variable when observing the field in the cavity by means of the atomic beam (see (3.9)). Defining  $\Delta x = 1/N$  and introducing the scaled probability distribution  $p(x) = Np_n$  the conservation of probability takes the form

$$\sum_{x=0}^{\infty} \Delta x \, p(x) = 1 , \quad (4.23)$$

where the sum extends over all discrete values of  $x$  in the interval. Similarly the equilibrium distribution takes the form

$$p^0(x) = \frac{1}{Z_x} e^{-NV(x)} , \quad (4.24)$$

with the effective potential given as an “integral”

$$V(x) = \sum_{x'>0}^x \Delta x' D(x') , \quad (4.25)$$

with “integrand”

$$D(x) = -\log \frac{n_b x + aq(x)}{(1+n_b)x + bq(x)} . \quad (4.26)$$

The transition probability function is  $q(x) = \sin^2 \theta \sqrt{x}$  and the normalization constant is given by

$$Z_x = \frac{Z}{N} = \sum_{x=0}^{\infty} \Delta x e^{-NV(x)} . \quad (4.27)$$

In order to reformulate the master equation (4.4) it is convenient to introduce the discrete derivatives  $\Delta_+ f(x) = f(x+\Delta x) - f(x)$  and  $\Delta_- f(x) = f(x) - f(x-\Delta x)$ . Then we find

$$\frac{1}{\gamma} \frac{dp(x)}{dt} = \frac{\Delta_+}{\Delta x} J(x) , \quad (4.28)$$

with

$$J(x) = (x - (a - b)q(x))p(x) + \frac{1}{N}(n_b x + aq(x))\frac{\Delta_-}{\Delta x}p(x) . \quad (4.29)$$

For the general eigenvector we define  $p(x) = Np_n$  and write it as  $p(x) = p^0(x)u(x)$  with  $u(x) = u_n$  and find the equations

$$\lambda p(x) = -\frac{\Delta_+}{\Delta x} J(x) , \quad (4.30)$$

and

$$J(x) = \frac{1}{N}p^0(x)((1+n_b)x + bq(x))\frac{\Delta_-}{\Delta x}u(x) . \quad (4.31)$$

Equivalently the eigenvalue equation for  $u(x)$  becomes

$$\lambda u(x) = (x - (a - b)q(x)) \frac{\Delta_-}{\Delta x} u(x) - \frac{1}{N} \frac{\Delta_+}{\Delta x} \left[ (n_b x + aq(x)) \frac{\Delta_-}{\Delta x} u(x) \right] . \quad (4.32)$$

As before we also have

$$\begin{aligned} \langle u(x) \rangle_0 &= 0 , \\ \langle u(x)^2 \rangle_0 &= 1 , \end{aligned} \quad (4.33)$$

where now the average over  $p^0(x)$  is defined as  $\langle f(x) \rangle_0 = \sum_x \Delta x f(x) p^0(x)$ . As before we may also express the eigenvalue as an average

$$\lambda = \frac{1}{N} \left\langle ((1 + n_b)x + b q(x)) \left( \frac{\Delta_- u(x)}{\Delta x} \right)^2 \right\rangle_0 . \quad (4.34)$$

Again it should be emphasized that all these formulas are exact rewritings of the previous ones, but this formulation permits easy transition to the continuum case, wherever applicable.

## 4.6 Extrema of the continuous potential

The quantity  $D(x)$  in Eq. (4.26) has a natural continuation to all real values of  $x$  as a smooth differentiable function. The condition for smoothness is that the change in the argument  $\theta\sqrt{x}$  between two neighbouring values,  $x$  and  $x + \Delta x$  is much smaller than 1, or  $\theta \ll 2N\sqrt{x}$ . Hence for  $N \rightarrow \infty$  the function is smooth everywhere and the sum in Eq. (4.25) may be replaced by an integral

$$V(x) = \int_0^x dx' D(x') , \quad (4.35)$$

so that  $D(x) = V'(x)$ . In Fig. 7 we illustrate the typical behaviour of the potential and the corresponding photon number distribution in the first critical region (see Section 5.6). Notice that the photon-number distribution exhibits Schleich-Wheeler oscillations typical of a squeezed state [43].

The extrema of this potential are located at the solutions to  $q(x) = x$ ; they may be parametrized in the form

$$\begin{aligned} x &= (a - b) \sin^2 \phi , \\ \theta &= \frac{1}{\sqrt{a - b}} \frac{\phi}{|\sin \phi|} , \end{aligned} \quad (4.36)$$

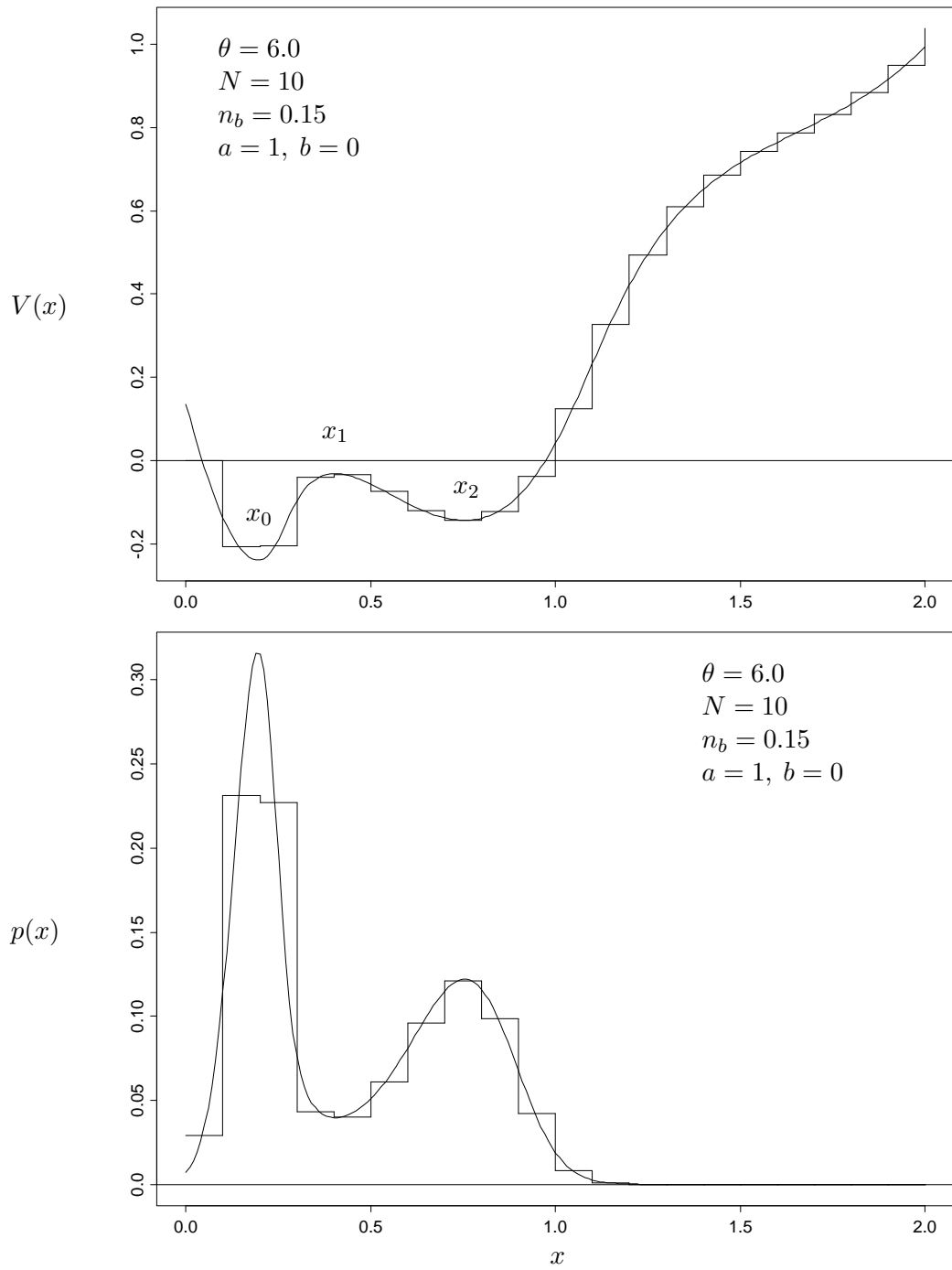


**Figure 7:** Example of a potential with two minima  $x_0, x_2$  and one maximum  $x_1$  (upper graph). The rectangular curve represents the exact potential (4.20), whereas the continuous curve is given by Eq. (4.25) with the summation replaced by an integral. The value of the continuous potential at  $x = 0$  has been chosen such as to make the distance minimal between the two curves. In the lower graph the corresponding probability distribution is shown.

with  $0 \leq \phi < \infty$ . These formulas map out a multibranched function  $x(\theta)$  with critical points where the derivative

$$D'(x) = V''(x) = \frac{(a + n_b(a - b))(q(x) - xq'(x))}{((1 + n_b)x + bq(x))(n_bx + aq(x))} \quad (4.37)$$

vanishes, which happens at the values of  $\phi$  satisfying  $\phi = \tan \phi$ . This equation has an infinity of solutions,  $\phi = \phi_k$ ,  $k = 0, 1, \dots$ , with  $\phi_0 = 0$  and to a good approximation

$$\phi_k = (2k + 1)\frac{\pi}{2} - \frac{1}{(2k + 1)\frac{\pi}{2}} + \mathcal{O}\left(\left((2k + 1)\frac{\pi}{2}\right)^{-3}\right) \quad (4.38)$$

for  $k = 1, 2, \dots$ , and each of these branches is double-valued, with a sub-branch corresponding to a minimum ( $D' > 0$ ) and another corresponding to a maximum ( $D' < 0$ ). Since there are always  $k + 1$  minima and  $k$  maxima, we denote the minima  $x_{2k}(\theta)$  and the maxima  $x_{2k+1}(\theta)$ . Thus the minima have even indices and the maxima have odd indices. They are given as a function of  $\theta$  through Eq. (4.36) when  $\phi$  runs through certain intervals. Thus, for the minima of  $V(x)$ , we have

$$\phi_k < \phi < (k + 1)\pi, \quad \theta_k < \theta < \infty, \quad a - b > x_{2k}(\theta) > 0, \quad k = 0, 1, \dots, \quad (4.39)$$

and for the maxima

$$k\pi < \phi < \phi_k, \quad \infty > \theta > \theta_k, \quad 0 < x_{2k+1}(\theta) < a - b, \quad k = 1, \dots \quad (4.40)$$

Here  $\theta_k = \phi_k / |\sin \phi_k| \sqrt{a - b}$  is the value of  $\theta$  for which the  $k$ 'th branch comes into existence. Hence in the interval  $\theta_K < \theta < \theta_{K+1}$  there are exactly  $2K + 1$  branches,  $x_0, x_1, x_2, \dots, x_{2K-1}, x_{2K}$ , forming the  $K + 1$  minima and  $K$  maxima of  $V(x)$ . For  $0 < \theta < \theta_0 = 1/\sqrt{a - b}$  there are no extrema.

This classification allows us to discuss the different parameter regimes that arise in the limit of  $N \rightarrow \infty$ . Each regime is separated from the others by singularities and are thus equivalent to the phases that arise in the thermodynamic limit of statistical mechanics.

## 5 Phase structure

We shall from now on limit the discussion to the case of initially completely excited atoms,  $a = 1$ ,  $b = 0$ , which simplifies the following discussion considerably.

The central issue in this paper is the phase structure of the correlation length as a function of the parameter  $\theta$ . In the limit of infinite atomic pumping rate,

$N \rightarrow \infty$ , the statistical system described by the master equation (2.10) has a number of different dynamical phases, separated from each other by singular boundaries in the space of parameters. We shall in this section investigate the character of the different phases, with special emphasis on the limiting behaviour of the correlation length. There turns out to be several qualitatively different phases within a range of  $\theta$  close to experimental values. First, the thermal phase and the transition to the maser phase at  $\theta = 1$  has previously been discussed in terms of  $\langle n \rangle$  [27, 41, 38]. The new transition to the critical phase at  $\theta_1 \simeq 4.603$  is not revealed by  $\langle n \rangle$  and the introduction of the correlation length as an observable is necessary to describe it. In the large flux limit  $\langle n \rangle$  and  $\langle (\Delta n)^2 \rangle$  are only sensitive to the probability distribution close to its global maximum. The correlation length depends crucially also on local maxima and the phase transition at  $\theta_1$  occurs when a new local maximum emerges. At  $\theta \simeq 6.3$  there is a phase transition in  $\langle n \rangle$  taking a discrete jump to a higher value. It happens when there are two competing global minima in the effective potential for different values of  $n$ . At the same point the correlation length reaches its maximum. In Fig. 8 we show the correlation length in the thermal and maser phases, and in Fig. 10 the critical phases, for various values of the pumping rate  $N$ .

## 5.1 Empty cavity

When there is no interaction, i.e.  $M = 1$ , or equivalently  $q_n = 0$  for all  $n$ , the behaviour of the cavity is purely thermal, and then it is possible to find the eigenvalues explicitly. Let us in this case write

$$L_C = (2n_b + 1)L_3 - (1 + n_b)L_- - n_bL_+ - \frac{1}{2} , \quad (5.1)$$

where

$$\begin{aligned} (L_3)_{nm} &= \left(n + \frac{1}{2}\right) \delta_{nm} , \\ (L_+)_n &= n\delta_{n,m+1} , \\ (L_-)_n &= (n + 1)\delta_{n+1,m} . \end{aligned} \quad (5.2)$$

These operators form a representation of the Lie algebra of  $SU(1,1)$

$$[L_-, L_+] = 2L_3 , \quad [L_3, L_\pm] = \pm L_\pm . \quad (5.3)$$

It then follows that

$$L_C = e^{rL_+} e^{-(1+n_b)L_-} (L_3 - \frac{1}{2}) e^{(1+n_b)L_-} e^{-rL_+} , \quad (5.4)$$

where  $r = n_b/(1 + n_b)$ . This proves that  $L_C$  has the same eigenvalue spectrum as the simple number operator  $L_3 - \frac{1}{2}$ , i.e.  $\lambda_n = n$  for  $n = 0, 1, \dots$ . Since  $M = 1$  for  $\tau = 0$  this is a limiting case for the correlation lengths  $\gamma\xi_n = 1/\lambda_n = 1/n$  for  $\theta = 0$ . From Eq. (4.8) we obtain  $\kappa_n = 1/(1 + n/N)$  in the non-interacting case. Hence in the discrete case  $R\xi_n = -1/\log \kappa_n \simeq N/n$  for  $N \gg n$  and this agrees with the values in Fig. 5 for  $n = 1, 2, 3$  near  $\tau = 0$ .

## 5.2 Thermal phase: $0 \leq \theta < 1$

In this phase the natural variable is  $n$ , not  $x = n/N$ . The effective potential has no extremum for  $0 < n < \infty$ , but is smallest for  $n = 0$ . Hence for  $N \rightarrow \infty$  it may be approximated by its leading linear term everywhere in this region

$$NV_n = n \log \frac{n_b + 1}{n_b + \theta^2} . \quad (5.5)$$

Notice that the slope vanishes for  $\theta = 1$ . The higher-order terms play no role as long as  $1 - \theta^2 \gg 1/\sqrt{N}$ , and we obtain a Planck distribution

$$p_n^0 = \frac{1 - \theta^2}{1 + n_b} \left( \frac{n_b + \theta^2}{1 + n_b} \right)^n , \quad (5.6)$$

with photon number average

$$\langle n \rangle = \frac{n_b + \theta^2}{1 - \theta^2} , \quad (5.7)$$

which (for  $\theta > 0$ ) corresponds to an increased temperature. Thus the result of pumping the cavity with the atomic beam is simply to raise its effective temperature in this region. The mean occupation number  $\langle n \rangle$  does not depend on the dimensionless pumping rate  $N$  (for sufficiently large  $N$ ).

The variance is

$$\sigma_n^2 = \langle n^2 \rangle - \langle n \rangle^2 = \langle n \rangle (1 + \langle n \rangle) = \frac{(1 + n_b)(n_b + \theta^2)}{(1 - \theta^2)^2} , \quad (5.8)$$

and the first non-leading eigenvector is easily shown to be

$$u_n = \frac{n - \langle n \rangle}{\sigma_n} , \quad (5.9)$$

which indeed has the form of a univariate variable. The corresponding eigenvalue is found from Eq. (4.34)  $\lambda_1 = 1 - \theta^2$ , or

$$\xi = \frac{1}{1 - \theta^2} . \quad (5.10)$$

Thus the correlation length diverges at  $\theta = 1$  (for  $N \rightarrow \infty$ ).

### 5.3 First critical point: $\theta = 1$

Around the critical point at  $\theta = 1$  there is competition between the linear and quadratic terms in the expansion of the potential for small  $x$

$$V(x) = x \log \frac{n_b + 1}{n_b + \theta^2} + \frac{1}{6} x^2 \frac{\theta^4}{\theta^2 + n_b} + \mathcal{O}(x^3) . \quad (5.11)$$

Expanding in  $\theta^2 - 1$  we get

$$V(x) = \frac{1 - \theta^2}{1 + n_b} x + \frac{1}{6(1 + n_b)} x^2 + \mathcal{O}(x^3, (\theta^2 - 1)^2) . \quad (5.12)$$

Near the critical point, i.e. for  $(1 - \theta^2)\sqrt{N} \ll 1$ , the quadratic term dominates, so the average value  $\langle x \rangle$  as well as the width  $\sigma_x$  becomes of  $\mathcal{O}(1/\sqrt{N})$  instead of  $\mathcal{O}(1/N)$ .

Let us therefore introduce two scaling variables  $r$  and  $\alpha$  through

$$x = r \sqrt{\frac{3(1 + n_b)}{N}}, \quad \theta^2 - 1 = \alpha \sqrt{\frac{1 + n_b}{3N}}, \quad (5.13)$$

so that the probability distribution in terms of these variables becomes a Gaussian on the half-line, i.e.

$$p^0(r) = \frac{1}{Z_r} e^{-\frac{1}{2}(r-\alpha)^2} \quad (5.14)$$

with

$$Z_r = \int_0^\infty dr e^{-\frac{1}{2}(r-\alpha)^2} = \sqrt{\frac{\pi}{2}} \left( 1 + \operatorname{erf} \left( \frac{\alpha}{\sqrt{2}} \right) \right) . \quad (5.15)$$

From this we obtain

$$\langle r \rangle = \alpha + \frac{d \log Z_r}{d\alpha}, \quad \sigma_r^2 = \frac{d \langle r \rangle}{d\alpha} . \quad (5.16)$$

For  $\alpha = 0$  we have explicitly

$$\langle x \rangle = \sqrt{\frac{12(1+n_b)}{\pi N}}, \quad \sigma_x^2 = \frac{6(n_b+1)}{N} \left( \frac{1}{2} - \frac{1}{\pi} \right) . \quad (5.17)$$

This leads to the following equation for  $u(r)$

$$\rho u = r(r-\alpha) \frac{du}{dr} - \frac{d}{dr} \left[ r \frac{du}{dr} \right] , \quad (5.18)$$

where

$$\rho = \lambda \sqrt{\frac{3N}{1+n_b}} = \left\langle r \left( \frac{du}{dr} \right)^2 \right\rangle_0 . \quad (5.19)$$

This eigenvalue problem has no simple solution.

We know, however, that  $u(r)$  must change sign once, say at  $r = r_0$ . In the neighbourhood of the sign change we have  $u \simeq r - r_0$  and, inserting this into (5.18) we get  $r_0 = (\alpha + \sqrt{4 + \alpha^2})/2$  and  $\rho = \sqrt{4 + \alpha^2}$  such that

$$\xi = \sqrt{\frac{3N}{(1+n_b)(4+\alpha^2)}} . \quad (5.20)$$

#### 5.4 Maser phase: $1 < \theta < \theta_1 \simeq 4.603$

In the region above the transition at  $\theta = 1$  the mean occupation number  $\langle n \rangle$  grows proportionally with the pumping rate  $N$ , so in this region the cavity acts as a maser. There is a single minimum of the effective potential described by the branch  $x_0(\theta)$ , defined by the region  $0 < \phi < \pi$  in Eq. (4.36). We find for  $N \gg 1$  to a good approximation in the vicinity of the minimum a Gaussian behaviour

$$p^0(x) = \sqrt{\frac{NV''(x_0)}{2\pi}} e^{-\frac{N}{2}V''(x_0)(x-x_0)^2} , \quad (5.21)$$

where

$$V''(x_0) = \frac{1 - q'(x_0)}{x_0(1+n_b)} . \quad (5.22)$$

Hence for  $(\theta^2 - 1)\sqrt{N} \gg 1$  we have a mean value  $\langle x \rangle_0 = x_0$  and variance  $\sigma_x^2 = 1/NV''(x_0)$ . To find the next-to-leading eigenvalue in this case we introduce the scaling variable  $r = \sqrt{NV''(x_0)}(x - x_0)$ , which has zero mean and unit variance for large  $N$ . Then Eq. (4.32) takes the form (in the continuum limit  $N \rightarrow \infty$ )

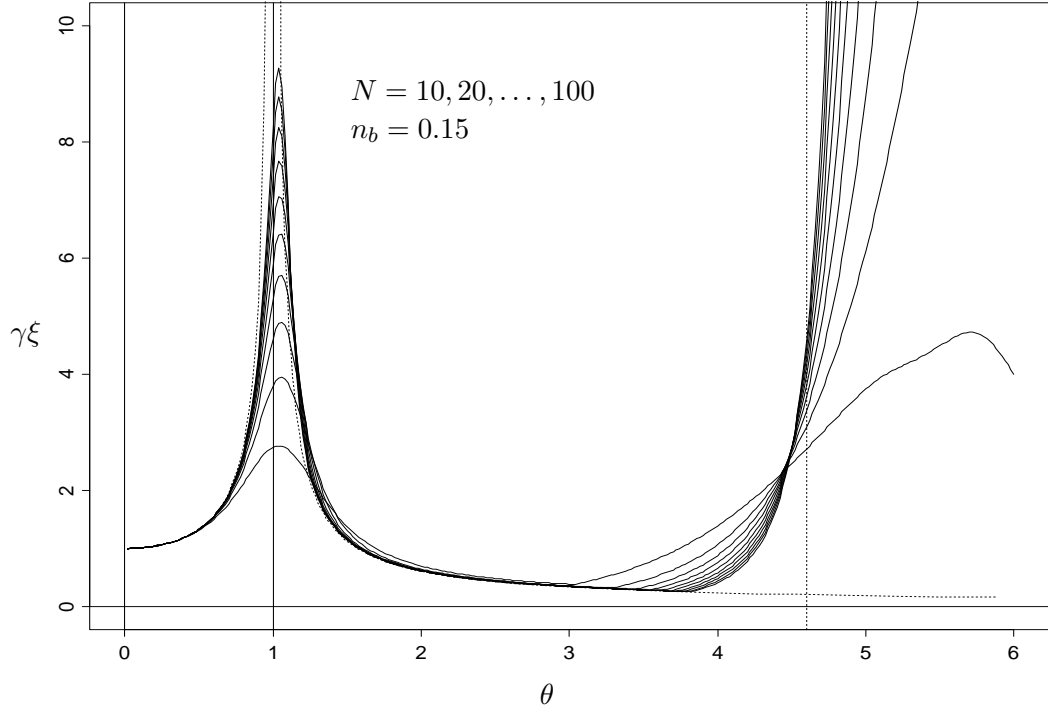


**Figure 8:** The correlation length in the thermal and maser phases as a function of  $\theta$  for various values of  $N$ . The dotted curves are the limiting value for  $N = \infty$ . The correlation length grows as  $\sqrt{N}$  near  $\theta = 1$  and exponentially for  $\theta > \theta_1 \simeq 4.603$ .

$$\lambda u = (1 - q'(x_0)) \left( r \frac{du}{dr} - \frac{d^2u}{dr^2} \right) . \quad (5.23)$$

This is the differential equation for Hermite polynomials. The eigenvalues are  $\lambda_n = n(1 - q'(x_0))$ ,  $n = 0, 1, \dots$ , and grow linearly with  $n$ . This may be observed in Fig. 4. The correlation length becomes

$$\xi = \frac{1}{1 - q'(x_0)} = \frac{1}{1 - \phi \cot \phi} \quad \text{for } 0 < \phi < \pi . \quad (5.24)$$

As in the thermal phase, the correlation length is independent of  $N$  (for large  $N$ ).

## 5.5 Mean field calculation

We shall now use a mean field method to get an expression for the correlation length in both the thermal and maser phases and in the critical region. We find from the time-dependent probability distribution (4.4) the following *exact* equation for the average photon occupation number:

$$\frac{1}{\gamma} \frac{d\langle n \rangle}{dt} = N\langle q_{n+1} \rangle + n_b - \langle n \rangle , \quad (5.25)$$

or with  $\Delta x = 1/N$

$$\frac{1}{\gamma} \frac{d\langle x \rangle}{dt} = \langle q(x + \Delta x) \rangle + n_b \Delta x - \langle x \rangle . \quad (5.26)$$

We shall ignore the fluctuations of  $x$  around its mean value and simply replace this by

$$\frac{1}{\gamma} \frac{d\langle x \rangle}{dt} = q(\langle x \rangle + \Delta x) + n_b \Delta x - \langle x \rangle . \quad (5.27)$$

This is certainly a good approximation in the limit of  $N \rightarrow \infty$  for the maser phase because the relative fluctuation  $\sigma_x/\langle x \rangle$  vanishes as  $\mathcal{O}(1/\sqrt{N})$  here, but it is of dubious validity in the thermal phase, where the relative fluctuations are independent of  $N$ . Nevertheless, we find numerically that the mean field description is rather precise in the whole interval  $0 < \theta < \theta_1$ .

The fixed point  $x_0$  of the above equation satisfies the mean field equation

$$x_0 = q(x_0 + \Delta x) + n_b \Delta x , \quad (5.28)$$

which may be solved in parametric form as

$$\begin{aligned} x_0 &= \sin^2 \phi + n_b \Delta x , \\ \theta &= \frac{\phi}{\sqrt{\sin^2 \phi + (1 + n_b) \Delta x}} . \end{aligned} \quad (5.29)$$

We notice here that there is a maximum region of existence for any branch of the solution. The maximum is roughly given by  $\theta_k^{\max} = (k + 1)\pi\sqrt{N/(1 + n_b)}$ .

For small perturbations  $\langle x \rangle = x_0 + \epsilon$  we find the equation of motion

$$\frac{1}{\gamma} \frac{d\epsilon}{dt} = -(1 - q'(x_0 + \Delta x))\epsilon , \quad (5.30)$$

from which we estimate the leading eigenvalue

$$\lambda = 1 - q'(x_0 + \Delta x) = 1 - \frac{\phi \sin \phi \cos \phi}{\sin^2 \phi + (1 + n_b) \Delta x} . \quad (5.31)$$

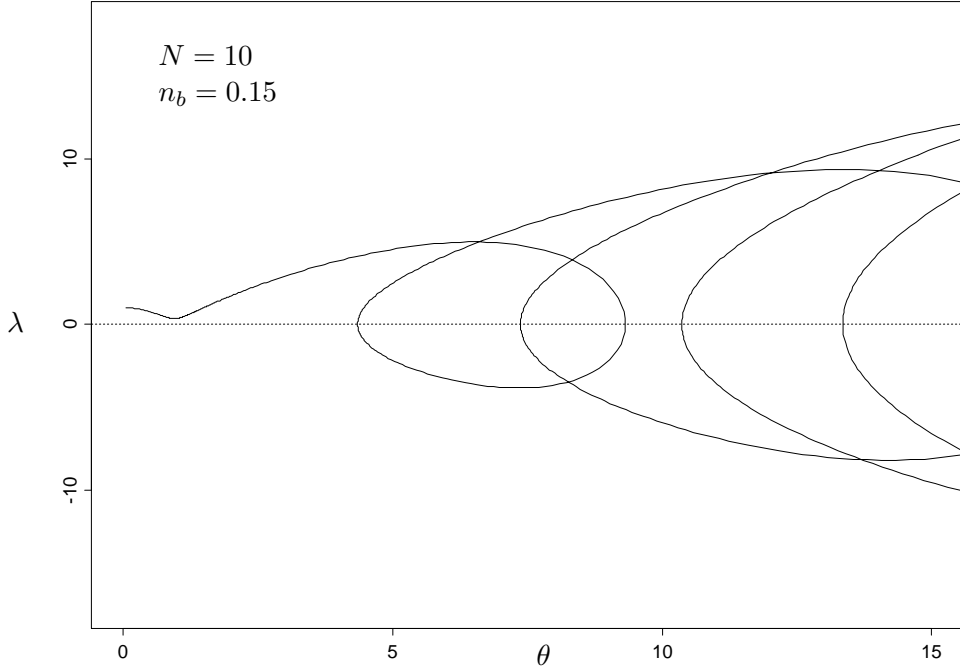


**Figure 9:** Mean field solution for the subleading eigenvalue.

In Fig. 9 this solution is plotted as a function of  $\theta$ . Notice that it takes negative values in the unstable regions of  $\phi$ . This eigenvalue does not vanish at the critical point  $\theta = 1$  which corresponds to

$$\phi \simeq \phi_0 = \left( \frac{3(1+n_b)}{N} \right)^{\frac{1}{4}} , \quad (5.32)$$

but only reaches a small value

$$\lambda \simeq 2\sqrt{\frac{1+n_b}{3N}} , \quad (5.33)$$

which agrees exactly with the previously obtained result (5.20). Introducing the scaling variable  $\alpha$  from (5.13) and defining  $\psi = (\phi/\phi_0)^2$  we easily get

$$\begin{aligned} \alpha &= (\psi^2 - 1)/\psi , \\ r &= \psi , \\ \rho &= (\psi^2 + 1)/\psi , \end{aligned} \quad (5.34)$$

and after eliminating  $\psi$

$$r = \frac{1}{2}(\alpha + \sqrt{\alpha^2 + 4}) \quad , \quad (5.35)$$

$$\rho = \sqrt{4 + \alpha^2} \quad ,$$

which agrees with the previously obtained results.

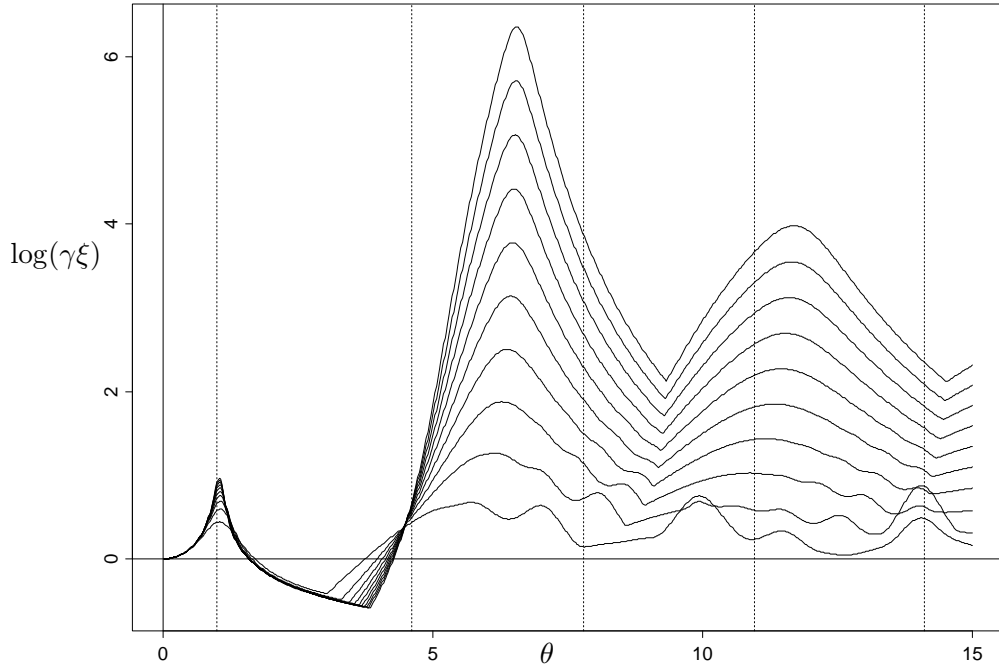


**Figure 10:** The logarithm of the correlation length as a function of  $\theta$  for various values of  $N$  ( $10, 20, \dots, 100$ ). We have  $n_b = 0.15$  here. Notice that for  $\theta > \theta_1$  the logarithm of the correlation length grows linearly with  $N$  for large  $N$ . The vertical lines indicate  $\theta_0 = 1$ ,  $\theta_1 = 4.603$ ,  $\theta_2 = 7.790$ ,  $\theta_3 = 10.95$  and  $\theta_4 = 14.10$ .

## 5.6 The first critical phase: $4.603 \simeq \theta_1 < \theta < \theta_2 \simeq 7.790$

We now turn to the first phase in which the effective potential has two minima ( $x_0, x_2$ ) and a maximum ( $x_1$ ) in between (see Fig. 7 in Section 4.6). In this case there is competition between the two minima separated by the barrier and for  $N \rightarrow \infty$  this barrier makes the relaxation time to equilibrium exponentially long. Hence we expect  $\lambda_1$  to be exponentially small for large  $N$  (see Fig. 10)

$$\lambda_1 = Ce^{-\eta N} \quad , \quad (5.36)$$

where  $C$  and  $\eta$  are independent of  $N$ . It is the extreme smallness of the subleading eigenvalue that allows us to calculate it with high precision.

For large  $N$  the probability distribution consists of two well-separated narrow maxima, each of which is approximately a Gaussian. We define the *a priori* probabilities for each of the peaks

$$P_0 = \sum_{0 \leq x < x_1} \Delta x \, p^0(x) = \frac{Z_0}{Z} , \quad (5.37)$$

and

$$P_2 = \sum_{x_1 \leq x < \infty} \Delta x \, p^0(x) = \frac{Z_2}{Z} . \quad (5.38)$$

The  $Z$ -factors are

$$Z_0 = \sum_{x=0}^{x_1} \Delta x \, e^{-NV(x)} \simeq e^{-NV_0} \sqrt{\frac{2\pi}{NV_0''}} , \quad (5.39)$$

and

$$Z_2 = \sum_{x=x_1}^{\infty} \Delta x \, e^{-NV(x)} \simeq e^{-NV_2} \sqrt{\frac{2\pi}{NV_2''}} , \quad (5.40)$$

with  $Z = Z_0 + Z_2$ . The probabilities satisfy of course  $P_0 + P_2 = 1$  and we have

$$p^0(x) = P_0 p_0^0(x) + P_2 p_2^0(x) , \quad (5.41)$$

where  $p_{0,2}^0$  are individual probability distributions with maximum at  $x_{0,2}$ . The overlap error in these expressions vanishes rapidly for  $N \rightarrow \infty$ , because the ratio  $P_0/P_2$  either converges towards 0 or  $\infty$  for  $V_0 \neq V_2$ . The transition from one peak being the highest to the other peak being the highest occurs when the two maxima coincide, i.e. at  $\theta \simeq 7.22$  at  $N = 10$ , whereas for  $N = \infty$  it happens at  $\theta \simeq 6.66$ . At this point the correlation length is also maximal.

Using this formalism, many quantities may be evaluated in the limit of large  $N$ . Thus for example

$$\langle x \rangle_0 = P_0 x_0 + P_2 x_2 , \quad (5.42)$$

and

$$\sigma_x^2 = \langle (x - \langle x \rangle_0)^2 \rangle_0 = \sigma_0^2 P_0 + \sigma_2^2 P_2 + (x_0 - x_2)^2 P_0 P_2 . \quad (5.43)$$

Now there is no direct relation between the variance and the correlation length.

Consider now the expression (4.30), which shows that since  $\lambda_1$  is exponentially small we have an essentially constant  $J_n$ , except near the maxima of the probability distribution, i.e. near the minima of the potential. Furthermore since the right eigenvector of  $\lambda_1$  satisfies  $\sum_x p(x) = 0$ , we have  $0 = J(0) = J(\infty)$  so that

$$J(x) \simeq \begin{cases} 0 & 0 < x < x_0 , \\ J_1 & x_0 < x < x_2 , \\ 0 & x_2 < x < \infty . \end{cases} \quad (5.44)$$

This expression is more accurate away from the minima of the potential,  $x_0$  and  $x_2$ .

Now it follows from Eq. (4.31) that the left eigenvector  $u(x)$  of  $\lambda_1$  must be constant, except near the minimum  $x_1$  of the probability distribution, where the derivative could be sizeable. So we conclude that  $u(x)$  is constant away from the maximum of the potential. Hence we must approximately have

$$u(x) \simeq \begin{cases} u_0 & 0 < x < x_1 , \\ u_2 & x_1 < x < \infty . \end{cases} \quad (5.45)$$

This expression is more accurate away from the maximum of the potential.

We may now relate the values of  $J$  and  $u$  by summing Eq. (4.30) from  $x_1$  to infinity

$$J_1 = J(x_1) = \lambda_1 \sum_{x=x_1}^{\infty} \Delta x p^0(x) u(x) \simeq \lambda_1 P_2 u_2 . \quad (5.46)$$

From Eq. (4.31) we get by summing over the interval between the minima

$$u_2 - u_0 = \frac{N J_1}{1 + n_b} \sum_{x=x_0}^{x_2} \Delta x \frac{1}{x p^0(x)} . \quad (5.47)$$

The inverse probability distribution has for  $N \rightarrow \infty$  a sharp maximum at the maximum of the potential. Let us define

$$Z_1 = \sum_{x=x_0}^{x_2} \Delta x \frac{1}{x} e^{N V(x)} \simeq \frac{1}{x_1} e^{N V_1} \sqrt{\frac{2\pi}{N(-V_1'')}} . \quad (5.48)$$

Then we find

$$u_2 - u_0 = \frac{N Z Z_1 J_1}{1 + n_b} = \frac{N \lambda_1 Z_1 Z_2 u_2}{1 + n_b} . \quad (5.49)$$

But  $u(x)$  must be univariate, i.e.

$$\begin{aligned} u_0 P_0 + u_2 P_2 &= 0 , \\ u_0^2 P_0 + u_2^2 P_2 &= 1 , \end{aligned} \tag{5.50}$$

from which we get

$$\begin{aligned} u_0 &= -\sqrt{\frac{P_2}{P_0}} = -\sqrt{\frac{Z_2}{Z_0}} , \\ u_2 &= \sqrt{\frac{P_0}{P_2}} = \sqrt{\frac{Z_0}{Z_2}} . \end{aligned} \tag{5.51}$$

Inserting the above solution we may solve for  $\lambda_1$

$$\lambda_1 = \frac{1+n_b}{N} \frac{Z_0 + Z_2}{Z_0 Z_1 Z_2} , \tag{5.52}$$

or more explicitly

$$\lambda_1 = \frac{x_1(1+n_b)}{2\pi} \sqrt{-V_1''} \left( \sqrt{V_0''} e^{-N(V_1-V_0)} + \sqrt{V_2''} e^{-N(V_1-V_2)} \right) . \tag{5.53}$$

Finally we may read off the coefficients  $\eta$  and  $C$  from Eq. (5.36). We get

$$\eta = \begin{cases} V_1 - V_0 & \text{for } V_0 > V_2 , \\ V_1 - V_2 & \text{for } V_2 > V_0 , \end{cases} \tag{5.54}$$

and

$$C = \frac{x_1(1+n_b)}{2\pi} \sqrt{-V_1''} \begin{cases} \sqrt{V_0''} & \text{for } V_0 > V_2 , \\ \sqrt{V_2''} & \text{for } V_2 > V_0 . \end{cases} \tag{5.55}$$

This expression is nothing but the result of a barrier penetration of a classical statistical process [52]. We have derived it in detail in order to get all the coefficients right.

It is interesting to check numerically how well Eq. (5.53) actually describes the correlation length. The coefficient  $\eta$  is given by Eq. (5.54), and we have numerically computed the highest barrier from the potential  $V(x)$  and compared it with an exact calculation in Fig. 11. The exponent  $\eta$  is extracted by comparing two values of the correlation length,  $\xi_{70}$  and  $\xi_{90}$ , for large values of  $N$  (70 and 90), where the difference in the prefactor  $C$  should be unimportant. The agreement between the two calculations is excellent when we use the exact potential. As a

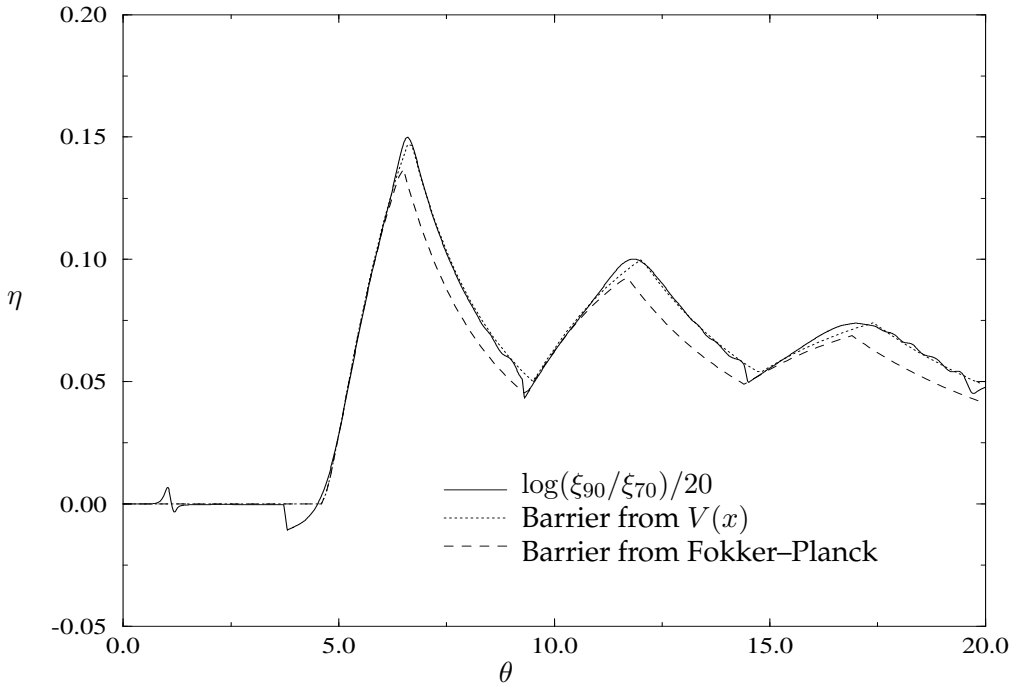


**Figure 11:** Comparing the barrier height from the potential  $V(x)$  with the exact correlation length and the barrier from an approximate Fokker–Planck formula.

comparison we also calculate the barrier height from the approximative potential in the Fokker–Planck equation derived in [27, 28]. We find a substantial deviation from the exact value in that case. It is carefully explained in [27, 28] why the Fokker–Planck potential cannot be expected to give a quantitatively correct result for small  $n_b$ . The exact result (solid line) has some extra features at  $\theta = 1$  and just below  $\theta = \theta_1 \simeq 4.603$ , due to finite-size effects.

When the first subleading eigenvalue goes exponentially to zero, or equivalently the correlation length grows exponentially, it becomes important to know the density of eigenvalues. If there is an accumulation of eigenvalues around 0, the long-time correlation cannot be determined by only the first subleading eigenvalue. It is quite easy to determine the density of eigenvalues simply by computing them numerically.

In Fig. 12 we show the first seven subleading eigenvalues for  $N = 50$  and  $n_b = 0.15$ . It is clear that at the first critical point after the maser phase ( $\theta = \theta_1$ ) there is only one eigenvalue going to zero. At the next critical phase ( $\theta = \theta_2$ ) there is one more eigenvalue coming down, and so on. We find that there is only one exponentially small eigenvalue for each new minimum in the potential, and thus there is no accumulation of eigenvalues around 0.

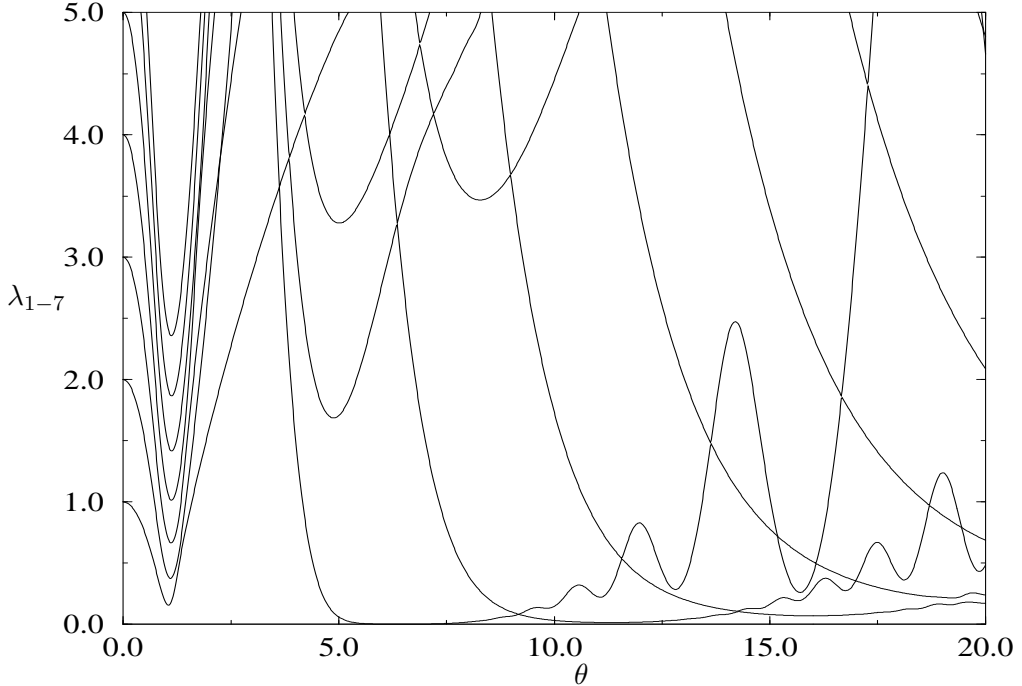


**Figure 12:** The first seven subleading eigenvalues for  $N = 50$  and  $n_b = 0.15$ .

## 6 Effects of velocity fluctuations

The time it takes an atom to pass through the cavity is determined by a velocity filter in front of the cavity. This filter is not perfect and it is relevant to investigate what a spread in flight time implies for the statistics of the interaction between cavity and beam. To be specific, we consider the flight time as an independent stochastic variable. Again, it is more convenient to work with the rescaled variable  $\vartheta$ , and we denote the corresponding stochastic variable by  $\vartheta$ . In order to get explicit analytic results we choose the following probability distribution for positive  $\vartheta$

$$f(\vartheta, \alpha, \beta) = \frac{\beta^{\alpha+1}}{\Gamma(\alpha+1)} \vartheta^\alpha e^{-\beta\vartheta} , \quad (6.1)$$

with  $\beta = \theta/\sigma_\theta^2$  and  $\alpha = \theta^2/\sigma_\theta^2 - 1$ , so that  $\langle \vartheta \rangle = \theta$  and  $\langle (\vartheta - \theta)^2 \rangle = \sigma_\theta^2$ . Other choices are possible, but are not expected to change the overall qualitative picture. The discrete master equation (2.19) for the equilibrium distribution can be averaged to yield

$$\langle p(t+T) \rangle = e^{-\gamma L_C T} \langle M(\vartheta) \rangle \langle p(t) \rangle , \quad (6.2)$$

The factorization is due to the fact that  $p(t)$  only depends on  $\vartheta$  for the preceding atoms, and that all atoms are statistically independent. The effect is simply to average  $q(\vartheta) = \sin^2(\vartheta\sqrt{x})$  in  $M(\vartheta)$ , and we get

$$\langle q \rangle = \frac{1}{2} \left[ 1 - \left( 1 + \frac{4x\sigma_\theta^4}{\theta^2} \right)^{-\frac{\theta^2}{2\sigma_\theta^2}} \cos \left( \frac{\theta^2}{\sigma_\theta^2} \arctan \left( \frac{2\sqrt{x}\sigma_\theta^2}{\theta} \right) \right) \right] . \quad (6.3)$$

This averaged form of  $q(\theta)$ , which depends on the two independent variables  $\theta/\sigma_\theta$  and  $\theta\sqrt{x}$ , enters in the analysis of the phases in exactly the same way as before. In the limit  $\sigma_\theta \rightarrow 0$  we regain the original  $q(\theta)$ , as we should. For very large  $\sigma_\theta$  and fixed  $\theta$ , and  $\langle q \rangle$  approaches zero.

## 6.1 Revivals and prerevivals

The phenomenon of quantum revival is an essential feature of the microlaser system (see [15]–[19], and [34]–[36]). The revivals are characterized by the reappearance of strongly oscillating structures in the excitation probability of an outgoing atom which is given by Eq. (3.1):

$$\mathcal{P}(+) = u^{0T} M(+) p^0 = \sum_n (1 - q_{n+1}(\theta)) p_n^0 , \quad (6.4)$$

where  $p_n^0$  is the photon distribution (2.23) in the cavity before the atom enters. Revivals occur when there is a resonance between the period in  $q_n$  and the discreteness in  $n$  [36]. If the photon distribution in the cavity has a sharp peak at  $n = n_0$  with a position that does not change appreciably when  $\theta$  changes, as for example for a fixed Poisson distribution, then it is easy to see that the first revival becomes pronounced in the region of  $\theta_{\text{rev}} \simeq 2\pi\sqrt{n_0 N}$ . For the equilibrium distribution without any spread in the velocities we do not expect any dramatic signature of revival, the reason being that the peaks in the equilibrium distribution  $p_n^0(\theta)$  move rapidly with  $\theta$ . In this context it is also natural to study the short-time correlation between two consecutive atoms, or the probability of finding two consecutive atoms in the excited level. This quantity is given by

$$\begin{aligned} \mathcal{P}_0(+, +) &= u^{0T} M(+) (1 + L_C/N)^{-1} M(+) p^0 \\ &= \sum_{n,m} (1 - q_{n+1}(\theta)) (1 + L_C/N)_{nm}^{-1} (1 - q_{m+1}(\theta)) p_m^0 , \end{aligned} \quad (6.5)$$

defined in Eq. (3.3). In Appendix C we give an analytic expression for the matrix elements of  $(1 + L_C/N)^{-1}$ . In Fig. 13 we present  $\mathcal{P}(+)$  and  $\mathcal{P}_0(+, +)$  for typical values of  $N$  and  $n_b$ .

If we on the other hand smear out the equilibrium distribution sufficiently as a function of  $\theta$ , revivals will again appear. The experimental situation we envisage

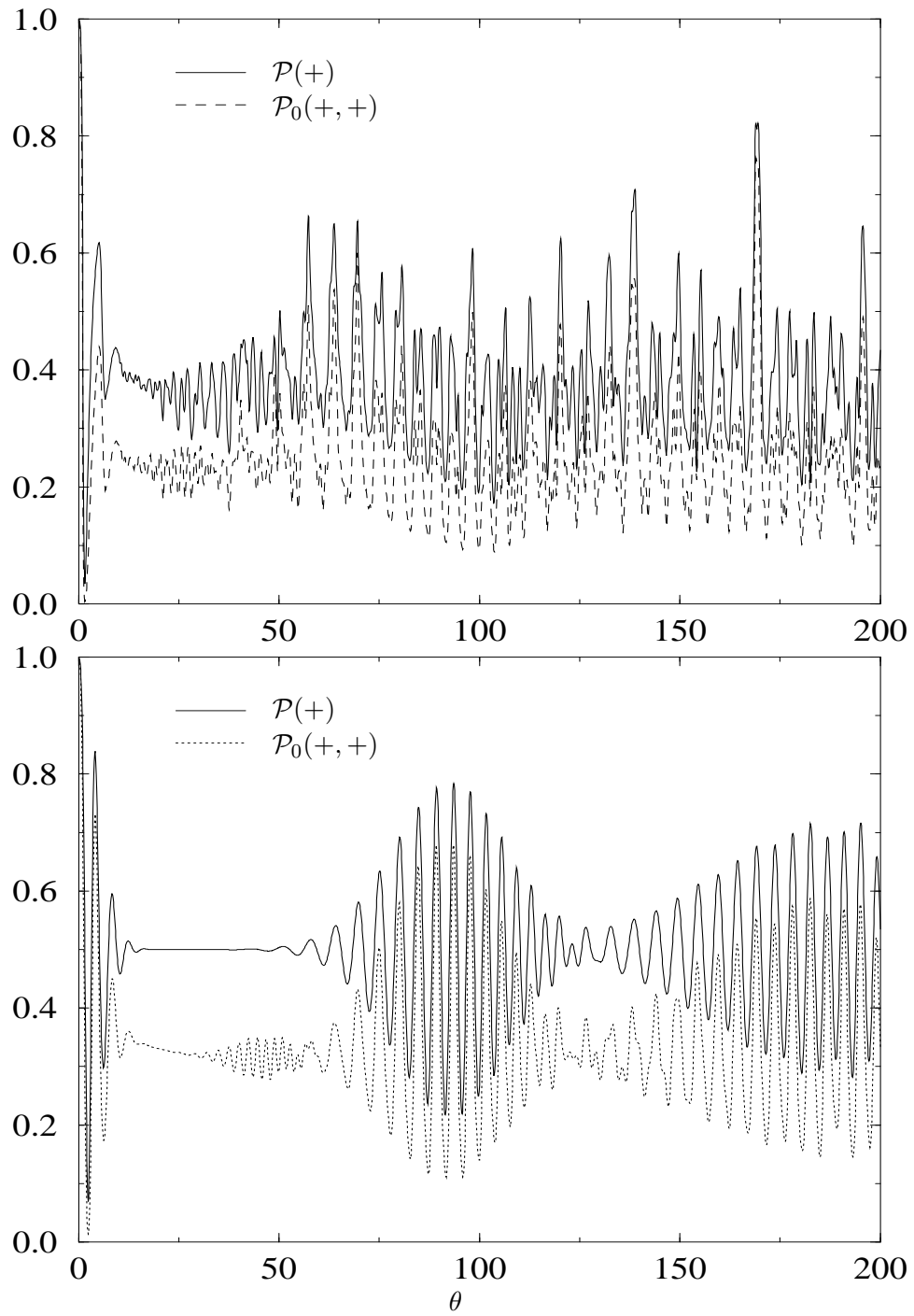


**Figure 13:** Upper graph: Probabilities of finding one atom, or two consecutive ones, in the excited state. The flux is given by  $N = 20$  and the thermal occupation number is  $n_b = 0.15$ . The curves show no evidence for the resonant behaviour of revivals. Lower graph: Presence of revival resonances in equilibrium after averaging the photon distribution over  $\theta$ . The same parameters as in Fig. 13 are used but the variance in  $\theta$  is now given by  $\sigma_\theta^2 = 10$ .

is that the atoms are produced with a certain spread in their velocities. The statistically averaged stationary photon distribution depends on the spread. After the passage through the cavity we measure both the excitation level and the speed of the atom. There is thus no averaging in the calculation of  $\mathcal{P}(+)$  and  $\mathcal{P}_0(+, +)$ , but these quantities now also depend on the actual value  $\vartheta$  for each atom. For definiteness we select only those atoms that fall in a narrow range around the average value  $\theta$ , in effect putting in a sharp velocity filter after the interaction. The result for an averaged photon distribution is presented in Fig. 13 (lower graph), where clear signs of revival are found. We also observe that in  $\mathcal{P}_0(+, +)$  there are *prerevivals*, occurring for a value of  $\theta$  half as large as for the usual revivals. Its origin is obvious since in  $\mathcal{P}_0(+, +)$  there are terms containing  $q_n^2$  that vary with the double of the frequency of  $q_n$ .

## 6.2 Phase diagram

The different phases discussed in Section 5 depend strongly on the structure of the effective potential. Averaging over  $\theta$  can easily change this structure and the phases. For instance, averaging with large  $\sigma_\theta$  would typically wash out some of the minima and lead to a different critical behaviour. We shall determine a two-dimensional phase diagram in the parameters  $\theta$  and  $\sigma_\theta$  by finding the lines where new minima occur and disappear. They are determined by the equations

$$\begin{aligned} \langle q \rangle &= x , \\ \frac{d\langle q \rangle}{dx} &= 1 . \end{aligned} \tag{6.6}$$

The phase boundary between the thermal and the maser phase is determined by the effective potential for small  $x$ . The condition  $\theta^2 = 1$  is now simply replaced by  $\langle \vartheta^2 \rangle = \theta^2 + \sigma_\theta^2 = 1$ , which also follows from the explicit form of  $\langle q \rangle$  in Eq. (6.3). The transitions from the maser phase to the critical phases are determined numerically and presented in Fig. 14. The first line starting from  $\theta \simeq 4.6$  shows where the second minimum is about to form, but exactly on this line it is only an inflection point. At the point  $a$  about  $\sigma_\theta \simeq 1.3$  it disappears, which occurs when the second minimum fuses with the first minimum. From the cusp at point  $a$  there is a new line (dashed) showing where the first minimum becomes an inflection point. Above the cusp at point  $a$  there is only one minimum. Going along the line from point  $b$  to  $c$  we thus first have one minimum, then a second minimum emerges, and finally the first minimum disappears before we reach point  $c$ . Similar things happens at the other cusps, which represent the fusing points for other minima. Thus, solid lines show where a new minimum emerges for large  $n$  ( $\sim N$ ) as  $\theta$  increases, while dashed lines show where a minimum disappears for small  $n$  as  $\sigma_\theta$  increases. We have also indicated (by dotted lines) the first-order maser

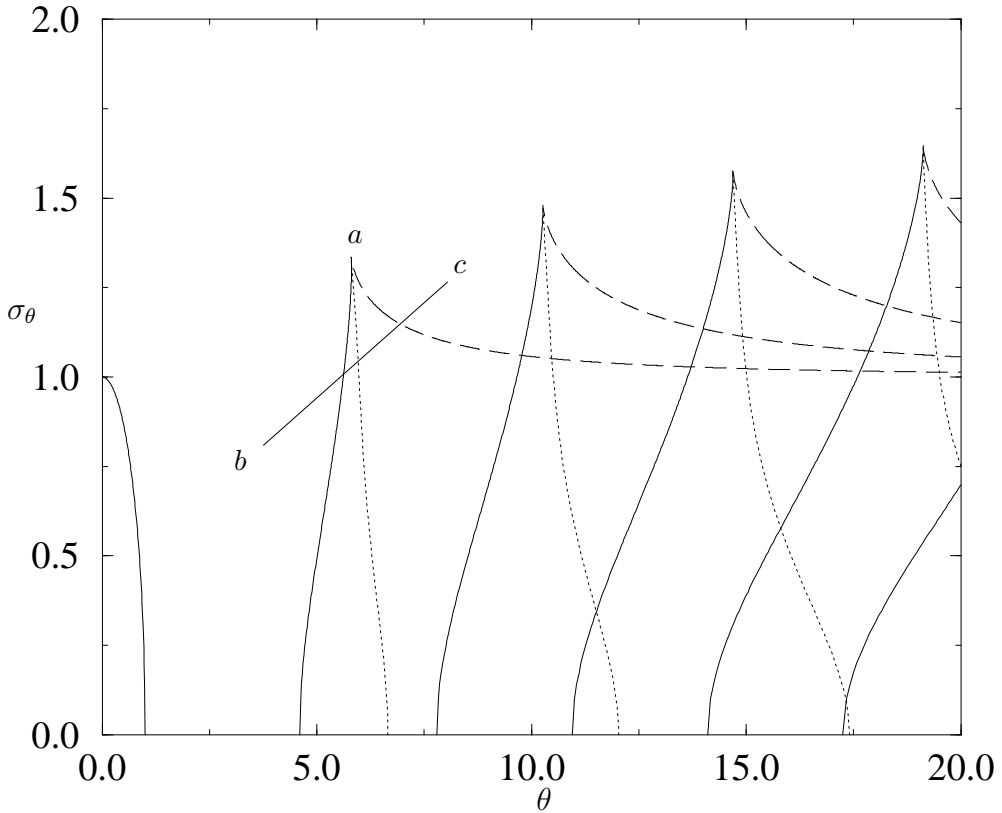


**Figure 14:** Phase diagram in the  $\theta-\sigma_\theta$  plane. The solid lines indicate where new minima in the effective potential emerge. In the lower left corner there is only one minimum at  $n = 0$ , this is the thermal phase. Outside that region there is always a minimum for non-zero  $n$  implying that the cavity acts as a maser. To the right of the solid line starting at  $\theta \simeq 4.6$ , and for not too large  $\sigma_\theta$ , there are two or more minima and thus the correlation length grows exponentially with the flux. For increasing  $\sigma_\theta$  minima disappear across the dashed lines, starting with those at small  $n$ . The dotted lines show where the two lowest minima are equally deep.

transitions where the two dominant minima are equally deep. These are the lines where  $\xi$  and  $Q_f$  have peaks and  $\langle n \rangle$  makes a discontinuous jump.

## 7 Finite-flux effects

So far, we have mainly discussed characteristics of the large flux limit. These are the defining properties for the different phases in Section 5. The parameter that controls finite flux effects is the ratio between the period of oscillations in the potential and the size of the discrete steps in  $x$ . If  $q = \sin^2(\theta\sqrt{x})$  varies slowly over  $\Delta x = 1/N$ , the continuum limit is usually a good approximation, while it can be very poor in the opposite case. In the discrete case there exist, for certain values of  $\theta$ , states that cannot be pumped above a certain occupation number since  $q_n = 0$

for that level. This effect is not seen in the continuum approximation. These states are called *trapping states* [51] and we discuss them and their consequences in this section.

The continuum approximation starts breaking down for small photon numbers when  $\theta \gtrsim 2\pi\sqrt{N}$ , and is completely inappropriate when the discreteness is manifest for all photon numbers lower than  $N$ , i.e. for  $\theta \gtrsim 2\pi N$ . In that case our analysis in Section 5 breaks down and the system may occasionally, for certain values of  $\theta$ , return to a non-critical phase.

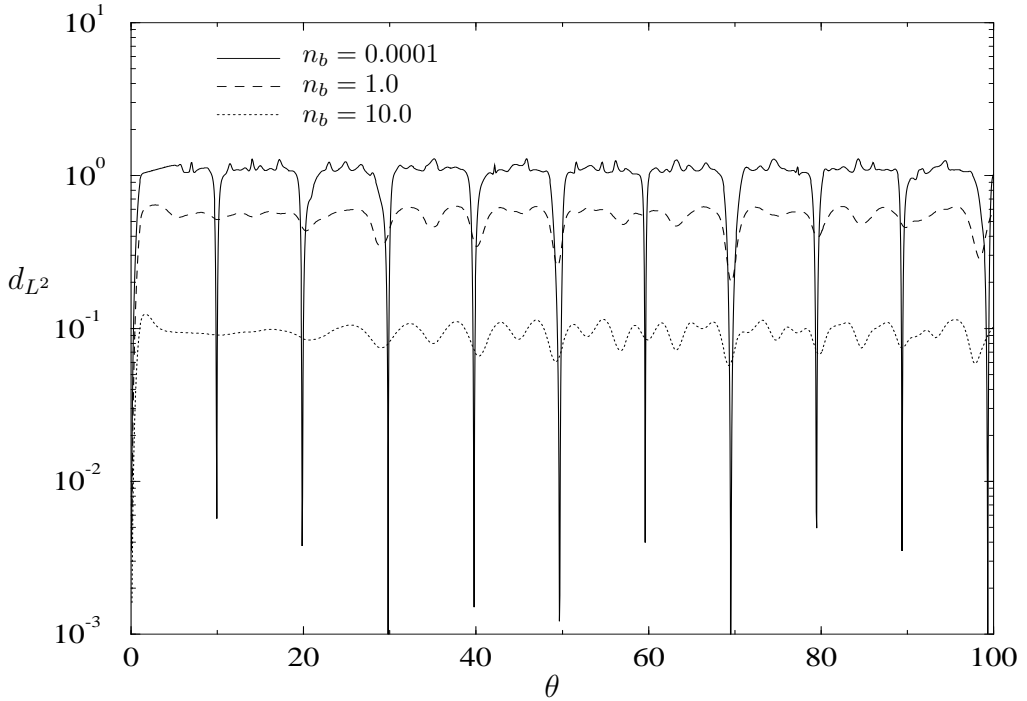


**Figure 15:** Distance between the initial probability distribution  $p_n(0)$  and  $p_n(\theta)$  measured by  $d_{L^2}(\theta)$  in Eq. (7.1).

## 7.1 Trapping states

The equilibrium distribution in Eq. (2.23) has peculiar properties whenever  $q_m = 0$  for some value of  $m$ , in particular when  $n_b$  is small, and dramatically so when  $n_b = 0$ . This phenomenon occurs when  $\theta = k\pi\sqrt{N/m}$  and is called a trapping state. When it happens, we have  $p_n = 0$  for all  $n \geq m$  (for  $n_b = 0$ ). The physics behind this can be found in Eq. (2.12), where  $M(-)$  determines the pumping of the cavity by the atoms. If  $q_m = 0$  the cavity cannot be pumped above  $m$  photons by emission from the passing atoms. For any non-zero value of  $n_b$  there is still a possibility for thermal fluctuation above  $m$  photons and  $p_n \neq 0$  even for  $n \geq m$ . The effect of trapping is lost in the continuum limit where the potential is approximated by Eq. (4.35). Some experimental consequences of trapping states

were studied for very low temperature in [50] and it was stated that in the range  $n_b = 0.1\text{--}1.0$  no experimentally measurable effects were present. We, however, show below that there are clear signals of trapping states in the correlation length even for  $n_b = 1.0$ .

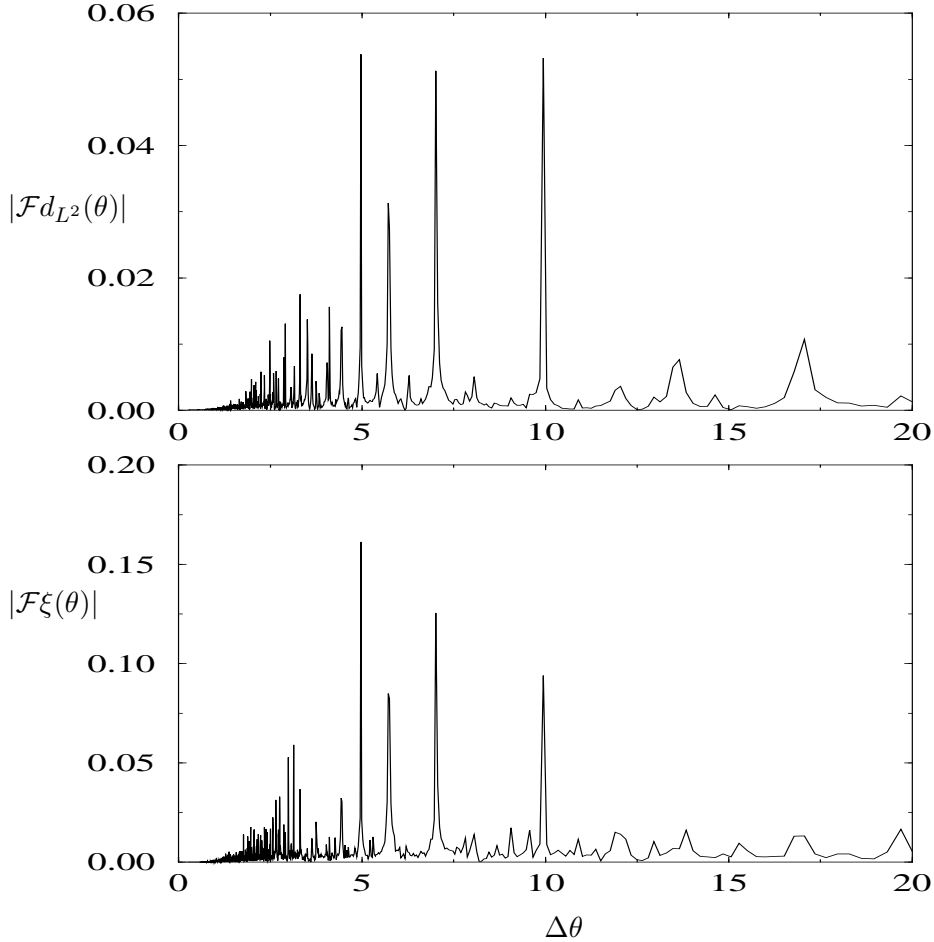


**Figure 16:** Amplitudes of Fourier modes of  $d_{L^2}(\theta)$  (upper graph) and  $\xi(\theta)$  (lower graph) as functions of periods using  $N = 10$ ,  $n_b = 1.0$  and scanning  $0 < \theta < 1024$ . There are pronounced peaks at the values of trapping states:  $\Delta\theta = \pi\sqrt{N/n}$ .

## 7.2 Thermal cavity revivals

Due to the trapping states, the cavity may revert to a statistical state, resembling the thermal state at  $\theta = 0$ , even if  $\theta > 0$ . By thermal revival we mean that the state of the cavity returns to the  $\theta = 0$  thermal state for other values of  $\theta$ . Even if the equilibrium state for non-zero  $\theta$  can resemble a thermal state, it does not at all mean that the dynamics at that value of  $\theta$  is similar to what it is at  $\theta = 0$ , since the deviations from equilibrium can have completely different properties.

A straightforward measure of the deviation from the  $\theta = 0$  state is the distance in the  $L^2$  norm

$$d_{L^2}(\theta) = \left( \sum_{n=0}^{\infty} [p_n(0) - p_n(\theta)]^2 \right)^{1/2}. \quad (7.1)$$

In Fig. 15 we exhibit  $d_{L^2}(\theta)$  for  $N = 10$  and several values of  $n_b$ .

For small values of  $n_b$  we find cavity revivals at all multiples of  $\sqrt{10\pi}$ , which can be explained by the fact that  $\sin(\theta\sqrt{n/N})$  vanishes for  $n = 1$  and  $N = 10$  at those points, i.e. the cavity is in a trapping state. That implies that  $p_n$  vanishes for  $n \geq 1$  (for  $n_b = 0$ ) and thus there are no photons in the cavity. For larger values of  $n_b$  the trapping is less efficient and the thermal revivals go away.

Going to much larger values of  $\theta$  we can start to look for periodicities in the fluctuations in  $d_{L^2}(\theta)$ . In Fig. 16 (upper graph) we present the spectrum of periods occurring in  $d_{L^2}(\theta)$  over the range  $0 < \theta < 1024$ .

Standard revivals should occur with a periodicity of  $\Delta\theta = 2\pi\sqrt{\langle n \rangle}$ , which is typically between 15 and 20, but there are hardly any peaks at these values. On the other hand, for periodicities corresponding to trapping states, i.e.  $\Delta\theta = \pi\sqrt{10/n}$ , there are very clear peaks, even though  $n_b = 1.0$ , which is a relatively large value.

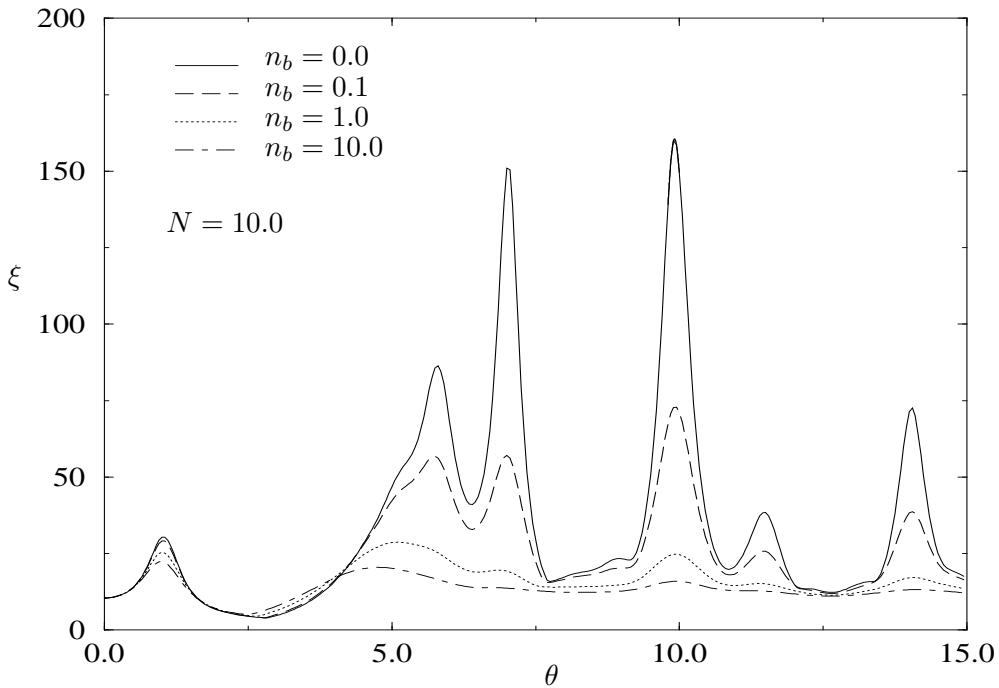


**Figure 17:** Correlation lengths for different values of  $n_b$ . The high peaks occur for trapping states and go away as  $n_b$  increases.

In order to see whether trapping states influence the correlation length we present in Fig. 16 a similar spectral decomposition of  $\xi(\theta)$  (lower graph) and we find the same peaks. A more direct way of seeing the effect of trapping states is to study the correlation length for small  $n_b$ . In Fig. 17 we see some very pronounced peaks for small  $n_b$  which rapidly go away when  $n_b$  increases. They are located at  $\theta = \pi k \sqrt{N/n}$  for every integer  $k$  and  $n$ . The effect is most dramatic when  $k$  is small. In Fig. 17 there are conspicuous peaks at  $\theta = \pi \sqrt{10} \cdot \{1/\sqrt{3}, 1/\sqrt{2}, 1, 2/\sqrt{3}, 2/\sqrt{2}\}$ , agreeing well with the formula for trapping states. Notice how sensitive the correlation length is to the temperature when  $n_b$  is small [50].

## 8 Conclusions

We have thoroughly discussed various aspects of long-time correlations in the micromaser. It is truly remarkable that this simple dynamical system can show such a rich structure of different phases. The two basic parameters in the theory are the time the atom spends in the cavity,  $\tau$ , and the ratio  $N = R/\gamma$  between the rate at which atoms arrive and the decay constant of the cavity. The natural observables are related to the statistics of the outgoing atom beam, the average excitation being the simplest one. We propose to use the long-time correlation length as a second observable describing different aspects of the photon statistics in the cavity. The phase structure we have investigated is defined in the limit of large flux, and can be summarized as follows:

- **Thermal phase,**  $0 \lesssim \theta < 1$ .

The mean number of photons  $\langle n \rangle$  is low (finite in the limit  $N \rightarrow \infty$ ), and so is the variance  $\sigma_n$  and the correlation length  $\xi$ .

- **Transition to maser phase,**  $\theta \simeq 1$ .

The maser is starting to get pumped up and  $\xi$ ,  $\langle n \rangle$ , and  $\sigma_n$  grow like  $\sqrt{N}$ .

- **Maser phase,**  $1 < \theta < \theta_1 \simeq 4.603$ .

The maser is pumped up to  $\langle n \rangle \sim N$ , but fluctuations remain smaller,  $\sigma_n \sim \sqrt{N}$ , whereas  $\xi$  is finite.

- **First critical phase,**  $\theta_1 < \theta < \theta_2 \simeq 7.790$ .

The correlation length increases exponentially with  $N$ , but nothing particular happens with  $\langle n \rangle$  and  $\sigma_n$  at  $\theta_1$ .

- **Second maser transition,**  $\theta \simeq 6.6$

As the correlation length reaches its maximum,  $\langle n \rangle$  makes a discontinuous jump to a higher value, though in both phases it is of the order of  $N$ . The fluctuations grow like  $N$  at this critical point.

At higher values of  $\theta$  there are more maser transitions in  $\langle n \rangle$ , accompanied by critical growth of  $\sigma_n$ , each time the photon distribution has two competing

maxima. The correlation length remains exponentially large as a function of  $N$ , as long as there are several maxima, though the exponential factor depends on the details of the photon distribution.

No quantum interference effects have been important in our analysis and the statistical aspects are purely classical. The reason is that we only study one atomic observable, the excitation level, which can take the values  $\pm 1$ . Making an analogy with a spin system, we can say that we only measure the spin along one direction. It would be very interesting to measure non-commuting variables, i.e. the spin in different directions or linear superpositions of an excited and decayed atom, and see how the phase transitions can be described in terms of such observables [40, 42]. Most effective descriptions of phase transitions in quantum field theory rely on classical concepts, such as the free energy and the expectation value of some field, and do not describe coherent effects. Since linear superpositions of excited and decayed atoms can be injected into the cavity, it therefore seems to be possible to study coherent phenomena in phase transitions both theoretically and experimentally, using the micromaser.

## Acknowledgements

B. L. and B.-S. S. wish to thank Gabriele Veneziano and the TH Division for the hospitality at CERN when this work was carried out and I. Lindgren for providing early guidance to the experimental work. The research by B.-S. S. was supported in part by the Swedish National Research Council under contract No. 8244-316, in part by the Research Council of Norway under contract No. 420.95/004. The research of B. L. was supported in part by the Danish Research Councils for the Natural and Technical Sciences through the Danish Computational Neural Network Center (CONNECT) under contracts No. 5.21.08.07 and 5.26.18.18.

## A Jaynes–Cummings with damping

In most experimental situations the time the atom spends in the cavity is small compared to the average time between the atoms and the decay time of the cavity. Then it is a good approximation to neglect the damping term when calculating the transition probabilities from the cavity–atom interaction. In order to establish the range of validity of the approximation we shall now study the full interaction governed by the JC Hamiltonian in Eq. (2.1) and the damping in Eq. (2.14). The density matrix for the cavity and one atom can be written as

$$\rho = \rho^0 \otimes \mathbb{1} + \rho^z \otimes \sigma_z + \rho^+ \otimes \sigma_- + \rho^- \otimes \sigma_+ , \quad (\text{A.1})$$

where  $\rho^\pm = \rho^x \pm i\rho^y$  and  $\sigma_\pm = (\sigma_x \pm i\sigma_y)/2$ . We want to restrict the cavity part of the density matrix to be diagonal, at least the  $\rho_0$  part, which is the only part of importance for the following atoms, provided that the first one is left unobserved (see discussion in Section 2.2). Introducing the notation

$$\begin{aligned} \rho_n^0 &= \langle n | \rho_0 | n \rangle , \\ \rho_n^z &= \langle n | \rho_z | n \rangle , \\ \rho_n^\pm &= \langle n | \rho_\pm | n - 1 \rangle - \langle n - 1 | \rho_\pm | n \rangle , \end{aligned} \quad (\text{A.2})$$

the equations of motion can be written as

$$\begin{aligned} \frac{d\rho_n^0}{dt} &= \frac{ig}{2}(\sqrt{n}\rho_n^\pm - \sqrt{n+1}\rho_{n+1}^\pm) - \gamma \sum_m L_{nm}^C \rho_m^0 , \\ \frac{d\rho_n^z}{dt} &= -\frac{ig}{2}(\sqrt{n}\rho_n^\pm + \sqrt{n+1}\rho_{n+1}^\pm) - \gamma \sum_m L_{nm}^C \rho_m^z , \\ \frac{d\rho_n^\pm}{dt} &= i2g\sqrt{n}(\rho_n^0 - \rho_{n-1}^0 - \rho_n^z - \rho_{n-1}^z) - \gamma \sum_m L_{nm}^\pm \rho_m^\pm , \end{aligned} \quad (\text{A.3})$$

where

$$\begin{aligned} L_{nm}^C &= [(n_b + 1)n + n_b(n + 1)]\delta_{n,m} - (n_b + 1)(n + 1)\delta_{n,m-1} - n_b n \delta_{n,m+1} , \\ L_{mn}^\pm &= [n_b(2n + 1) - \frac{1}{2}]\delta_{n,m} - (n_b + 1)\sqrt{n(n + 1)}\delta_{n,m-1} - n_b\sqrt{n(n - 1)}\delta_{n,m+1} . \end{aligned} \quad (\text{A.4})$$

It is thus consistent to study the particular form of the cavity density matrix, which has only one non-zero diagonal or subdiagonal for each component, even

when damping is included. Our strategy shall be to calculate the first-order correction in  $\gamma$  in the interaction picture, using the JC Hamiltonian as the free part. The JC part of Eq. (A.3) can be drastically simplified using the variables

$$\begin{aligned}\rho_n^s &= \rho_0^n + \rho_0^{n-1} - \rho_z^n + \rho_z^{n-1} , \\ \rho_n^a &= \rho_0^n - \rho_0^{n-1} - \rho_z^n - \rho_z^{n-1} .\end{aligned}\quad (\text{A.5})$$

The equations of motion then take the form

$$\begin{aligned}\frac{d\rho_n^s}{dt} &= -\frac{\gamma}{2} \sum_m \left[ (L_{nm}^C + L_{n-1,m-1}^C) \rho_m^s + (L_{nm}^C - L_{n-1,m-1}^C) \rho_m^a \right] , \\ \frac{d\rho_n^a}{dt} &= 2ig\sqrt{n} \rho_n^\pm - \frac{\gamma}{2} \sum_m \left[ (L_{nm}^C - L_{n-1,m-1}^C) \rho_m^s + (L_{nm}^C + L_{n-1,m-1}^C) \rho_m^a \right] , \\ \frac{d\rho_n^\pm}{dt} &= 2ig\sqrt{n} \rho_n^a - \gamma \sum_m L_{nm}^\pm \rho_m^\pm .\end{aligned}\quad (\text{A.6})$$

The initial conditions  $\rho_n^s(0) = p_{n-1}$ ,  $\rho_n^a(0) = -p_{n-1}$  and  $\rho_n^\pm(0) = 0$  are obtained from

$$\begin{aligned}\text{Tr}(\rho(0)|n\rangle\langle n| \otimes \mathbb{1}) &= 2\rho_0^n(0) = p_n , \\ \text{Tr}\left(\rho(0)|n\rangle\langle n| \otimes \frac{1}{2}(\mathbb{1} - \sigma_z)\right) &= \rho_0^n(0) - \rho_z^n(0) = 0 , \\ \text{Tr}(\rho(0)|n\rangle\langle n| \otimes \sigma_x) &= \text{Tr}(\rho(0)|n\rangle\langle n| \otimes \sigma_y) = 0 .\end{aligned}\quad (\text{A.7})$$

In the limit  $\gamma \rightarrow 0$  it is easy to solve Eq. (A.6) and we get back the standard solution of the JC equations, which is

$$\begin{aligned}\rho_s^n(t) &= p_{n-1} , \\ \rho_a^n(t) &= -p_{n-1} \cos(2gt\sqrt{n}) , \\ \rho_\pm^n(t) &= -ip_{n-1} \sin(2gt\sqrt{n}) .\end{aligned}\quad (\text{A.8})$$

Equation (A.6) is a matrix equation of the form  $\dot{\rho} = (C_0 - \gamma C_1)\rho$ . When  $C_0$  and  $C_1$  commute the solution can be written as  $\rho(t) = \exp(\gamma C_1 t) \exp(C_0 t) \rho(0)$ , which is the expression used in Eq. (2.19). In our case  $C_0$  and  $C_1$  do not commute and we have to solve the equations perturbatively in  $\gamma$ . Let us write the solution as  $\rho(t) = \exp(C_0 t) \rho_1(t)$  since  $\exp(C_0 t)$  can be calculated explicitly. The equation for  $\rho_1(t)$  becomes

$$\frac{d\rho_1}{dt} = -\gamma e^{-C_0 t} C_1 e^{C_0 t} \rho_1(t) , \quad (\text{A.9})$$

which to lowest order in  $\gamma$  can be integrated as

$$\rho_1(\tau) = -\gamma \int_0^\tau dt e^{-C_0 t} C_1 e^{C_0 t} \rho(0) + \rho(0) . \quad (\text{A.10})$$

The explicit expression for  $\exp(C_0 t)$  is

$$e^{C_0 t} = \delta_{nm} \begin{pmatrix} 1 & 0 & 0 \\ 0 & \cos(2gt\sqrt{n}) & i \sin(2gt\sqrt{n}) \\ 0 & i \sin(2gt\sqrt{n}) & \cos(2gt\sqrt{n}) \end{pmatrix} , \quad (\text{A.11})$$

and, therefore,  $\exp(-C_0 t) C_1 \exp(C_0 t)$  is a bounded function of  $t$ . The elements of  $C_1$  are given by various combinations of  $L_{nm}^C$  and  $L_{nm}^\pm$  in Eq. (A.4) and they grow at most linearly with the photon number. Thus the integrand of Eq. (A.10) is of the order of  $\langle n \rangle$  up to an  $n_b$ -dependent factor. We conclude that the damping is negligible as long as  $\gamma\tau\langle n \rangle \ll 1$ , unless  $n_b$  is very large. When the cavity is in a maser phase,  $\langle n \rangle$  is of the same order of magnitude as  $N = R/\gamma$ , so the condition becomes  $\tau R \ll 1$ .

## B Sum rule for the correlation lengths

In this appendix we derive the sum rule quoted in Eq. (3.14) and use the notation of Section 4.3.

For  $A_K = 0$  the determinant  $\det L_K$  becomes  $B_0 B_1 \cdots B_K$  as may be easily derived by row manipulation. Since  $A_K$  only occurs linearly in the determinant it must obey the recursion relation  $\det L_K = B_0 \cdots B_K + A_K \det L_{K-1}$ . Repeated application of this relation leads to the expression

$$\det L_K = \sum_{k=0}^{K+1} B_0 \cdots B_{k-1} A_k \cdots A_K . \quad (\text{B.1})$$

This is valid for arbitrary values of  $B_0$  and  $A_K$ . Notice that here we define  $B_0 \cdots B_{k-1} = 1$  for  $k = 0$  and similarly  $A_k \cdots A_K = 1$  for  $k = K+1$ .

In the actual case we have  $B_0 = A_K = 0$ , so that the determinant vanishes. The characteristic polynomial consequently takes the form

$$\det(L_K - \lambda) = (-\lambda)(\lambda_1 - \lambda) \cdots (\lambda_K - \lambda) = -D_1\lambda + D_2\lambda^2 + \mathcal{O}(\lambda^3) , \quad (\text{B.2})$$

where the last expression is valid for  $\lambda \rightarrow 0$ . The coefficients are

$$D_1 = \lambda_1 \cdots \lambda_K , \quad (\text{B.3})$$

and

$$D_2 = D_1 \sum_{k=1}^K \frac{1}{\lambda_k} . \quad (\text{B.4})$$

To calculate  $D_1$  we note that it is the sum of the  $K$  subdeterminants along the diagonal. The subdeterminant obtained by removing the  $k$ 'th row and column takes the form

$$\left| \begin{array}{ccc} A_0 + B_0 & -B_1 & \\ & \vdots & \\ -A_{k-2} & A_{k-1} + B_{k-1} & 0 \\ & 0 & A_{k+1} + B_{k+1} & -B_{k+2} \\ & & \vdots & \\ & & -A_{K-1} & A_K + B_K \end{array} \right| , \quad (\text{B.5})$$

which decomposes into the product of two smaller determinants which may be calculated using Eq. (B.1). Using that  $B_0 = A_K = 0$  we get

$$D_1 = \sum_{k=0}^K A_0 \cdots A_{k-1} B_{k+1} \cdots B_K . \quad (\text{B.6})$$

Repeating this procedure for  $D_2$  which is a sum of all possible diagonal subdeterminants with two rows and columns removed ( $0 \leq k < l \leq K$ ), we find

$$D_2 = \sum_{k=0}^{K-1} \sum_{l=k+1}^K \sum_{m=k+1}^l A_0 \cdots A_{k-1} B_{k+1} \cdots B_{m-1} A_m \cdots A_{l-1} B_{l+1} \cdots B_K . \quad (\text{B.7})$$

Finally, making use of Eq. (4.13) we find

$$D_1 = \frac{B_1 \cdots B_K}{p_0^0} \sum_{k=0}^K p_k^0 , \quad (\text{B.8})$$

and

$$D_2 = \frac{B_1 \cdots B_K}{p_0^0} \sum_{k=0}^{K-1} \sum_{l=k+1}^K \sum_{m=k+1}^l \frac{p_k^0 p_l^0}{B_m p_m^0} . \quad (\text{B.9})$$

Introducing the cumulative probability

$$P_n^0 = \sum_{m=0}^{n-1} p_m^0 , \quad (\text{B.10})$$

and interchanging the sums, we get the correlation sum rule

$$\sum_{n=1}^K \frac{1}{\lambda_n} = \sum_{n=1}^K \frac{P_n^0(1 - P_n^0/P_{K+1}^0)}{B_n p_n^0} . \quad (\text{B.11})$$

This sum rule is valid for finite  $K$  but diverges for  $K \rightarrow \infty$ , because the equilibrium distribution  $p_n^0$  approaches a thermal distribution for  $n \gg N$ . Hence the right-hand side diverges logarithmically in that limit. The left-hand side also diverges logarithmically with the truncation size because we have  $\lambda_n^0 = n$  for the untruncated thermal distribution. We do not know the thermal eigenvalues for the truncated case, but expect that they will be of the form  $\lambda_n^0 = n + \mathcal{O}(n^2/K)$  since they should vanish for  $n = 0$  and become progressively worse as  $n$  approaches  $K$ . Such a correction leads to a finite correction to  $\sum_n 1/\lambda_n$ . In fact, evaluating the right-hand side of Eq. (B.11), we get for large  $K$

$$\sum_{n=1}^K \frac{1}{\lambda_n^0} \simeq \sum_{n=1}^K \frac{1 - [n_b/(1 + n_b)]^n}{n} \simeq \sum_{n=1}^K \frac{1}{n} - \log(1 + n_b) . \quad (\text{B.12})$$

Subtracting the thermal case from Eq. (B.11) we get in the limit of  $K \rightarrow \infty$

$$\sum_{n=1}^{\infty} \left( \frac{1}{\lambda_n} - \frac{1}{\lambda_n^0} \right) = \sum_{n=1}^{\infty} \left( \frac{P_n^0(1 - P_n^0)}{B_n p_n^0} - \frac{1 - [n_b/(1 + n_b)]^n}{n} \right) . \quad (\text{B.13})$$

Here we have extended the summation to infinity under the assumption that for large  $n$  we have  $\lambda_n \simeq \lambda_n^0$ . The left-hand side can be approximated by  $\xi - 1$  in regions where the leading correlation length is much greater than the others. A comparison of the exact eigenvalue and the sum-rule prediction is made in Fig. 6.

## C Damping matrix

In this appendix we find an integral representation for the matrix elements of  $(x + L_C)^{-1}$ , where  $L_C$  is given by Eq. (2.18). Let

$$v_n = \sum_{m=0}^{\infty} (x\delta_{nm} + (L_C)_{nm})w_m , \quad (\text{C.1})$$

and introduce generating functionals  $v(z)$  and  $w(z)$  for complex  $z$  defined by

$$v(z) = \sum_{n=0}^{\infty} z^n v_n , \quad w(z) = \sum_{n=0}^{\infty} z^n w_n . \quad (\text{C.2})$$

By making use of

$$v(z) = \sum_{n,m=0}^{\infty} (x + L_C)_{nm} z^n w_m \quad , \quad (\text{C.3})$$

one can derive a first-order differential equation for  $w(z)$ ,

$$(x + n_b(1 - z))w(z) + (1 + n_b(1 - z))(z - 1) \frac{dw(z)}{dz} = v(z) \quad , \quad (\text{C.4})$$

which can be solved with the initial condition  $v(1) = 1$ , i.e.  $w(1) = 1/x$ . If we consider the monomial  $v(z) = v_m z^m$  and the corresponding  $w(z) = w_m(z)$ , we find that

$$w_m(z) = \int_0^1 dt (1-t)^{x-1} \frac{[z(1-t(1+n_b)) + t(1+n_b)]^m}{[1+n_bt(1-z)]^{m+1}} \quad . \quad (\text{C.5})$$

Therefore  $(x + L_C)_{nm}^{-1}$  is given by the coefficient of  $z^n$  in the series expansion of  $w_m(z)$ . In particular, we obtain for  $n_b = 0$  the result

$$(x + L_C)_{nm}^{-1} = \binom{m}{n} \frac{\Gamma(x+n)\Gamma(m-n+1)}{\Gamma(x+m+1)} \quad , \quad (\text{C.6})$$

where  $m \geq n$ . We then find that

$$\mathcal{P}_0(+,+) = \sum_{n=0}^{\infty} \cos^2(g\tau\sqrt{n+1}) \sum_{m=n}^{\infty} \frac{m!}{n!} \frac{N\Gamma(N+n)}{\Gamma(N+m+1)} \cos^2(g\tau\sqrt{m+1}) p_m^0 \quad , \quad (\text{C.7})$$

where  $p_m^0$  is the equilibrium distribution given by Eq. (2.23), and where  $x = N = R/\gamma$ . Equation (C.7) can also be derived from the known solution of the master equation in Eq. (2.14) for  $n_b = 0$  [44]. For small  $n_b$  and/or large  $x$ , Eq. (C.5) can be used to find a series expansion in  $n_b$ .

## References

- [1] P. Goy, J. M. Raimond, M. Gross and S. Haroche, *Observation of cavity-enhanced single-atom spontaneous emission*, Phys. Rev. Lett. **50** (1983) 1903.
- [2] D. Meschede, H. Walther and G. Müller, *One-atom maser*, Phys. Rev. Lett. **54** (1985) 551.
- [3] H. Walther, *The single atom maser and the quantum electrodynamics in a cavity*, Physica Scripta **T23** (1988) 165.
- [4] H. Walther, *Experiments on cavity quantum electrodynamics*, Phys. Rep. **219** (1992) 263.
- [5] H. Walther, *Experiments with single atoms in cavities and traps*, in *Fundamental problems in quantum theory*, Eds. D. M. Greenberger and A. Zeiler, Ann. N.Y. Acad. Sci. **755** (1995) 133.
- [6] K. An, J. J. Childs, R. R. Dasari, and M. S. Feld, *Microlaser: A laser with one atom in an optical resonator*, Phys. Rev. Lett. **73** (1994) 3375.
- [7] S. Haroche, *Cavity quantum electrodynamics*, in *Fundamental systems in quantum optics*, Eds. J. Dalibard, J. M. Raimond and J. Zinn-Justin, (Elsevier, 1992).
- [8] D. Meschede, *Radiating atoms in confined space: From spontaneous emission to micromasers*, Phys. Rep. **211** (1992) 201.
- [9] P. Meystre, *Cavity quantum optics and the quantum measurement process*, *Progress in Optics XXX*, p. 261, Ed. E. Wolf, (Elsevier, 1992).
- [10] E. I. Aliskenderov, A. S. Shumovsii and H. Trung Dung, *Quantum effects in the interaction of an atom with radiation*, Phys. Part. Nucl. **24** (1993) 177.
- [11] A. N. Oraevskii, *Spontaneous emission in a cavity*, Physics Uspekhi **37** (1994) 393.
- [12] S. M. Barnett, F. Filipowicz, J. Javanainen, P. L. Knight and P. Meystre, *The Jaynes-Cummings model and beyond*, in *Frontiers in quantum optics*, Eds. E. R. Pike and S. Sarkar, (Adam Bilger, 1986).
- [13] P. W. Milonni and S. Singh, *Some recent developments in the fundamental theory of light*, in *Advances in atomic, molecular, and optical physics* **28** (1991) 75, Eds. D. Bates and B. Bederson, (Academic Press, 1991).
- [14] E. T. Jaynes and F. W. Cummings, *Comparison of quantum and semiclassical radiation theories with application to the beam maser*, Proc. IEEE **51** (1963) 89.
- [15] P. Meystre, E. Geneux, A. Quattropani and A. Faist, *Long-time behaviour of a two-level system in interaction with an electromagnetic field*, Nuovo Cimento **25B** (1975) 521.

- [16] J. H. Eberly, N. B. Narozhny and J. J. Sanchez-Mondragon, *Periodic spontaneous collapse and revival in a simple quantum model*, Phys. Rev. Lett. **44** (1980) 1323.
- [17] N. B. Narozhny, J. J. Sanchez-Mondragon and J. H. Eberly, *Coherence versus incoherence: Collapse and revival in a simple quantum model*, Phys. Rev. **A23** (1981) 236.
- [18] P. L. Knight and P. M. Radmore, *Quantum revivals of a two-level system driven by chaotic radiation*, Phys. Lett. **90A** (1982) 342.
- [19] P. Filipowicz, *Quantum revivals in the Jaynes-Cummings model*, J. Phys. A: Math. Gen. **19** (1986) 3785.
- [20] G. Arroyo-Correa and J. J. Sanchez-Mondragon, *The Jaynes-Cummings model thermal revivals*, Quantum Opt. **2** (1990) 409.
- [21] G. Rempe, H. Walther and N. Klein, *Observation of quantum collapse and revival in a one-atom maser*, Phys. Rev. Lett. **58** (1987) 353.
- [22] R. Hanbury-Brown and R. Q. Twiss, *Correlation between photons in two coherent beams of light*, Nature **177** (1956) 27.
- [23] R. J. Glauber, *The quantum theory of optical coherence*, Phys. Rev. **130** (1963) 2529.
- [24] D. H. Boal, C.-K. Gelbke and B. K. Jennings, *Intensity interferometry in subatomic physics*, Rev. Mod. Phys. **62** (1990) 553.
- [25] B.-S. Skagerstam, *Coherent states — Some applications in quantum field theory and particle physics*, in *Coherent states: Past, present, and the future*, p. 469, Eds. D. H. Feng, J. R. Klauder and M. R. Strayer, (World Scientific, 1994).
- [26] P. Elmfors, B. Lautrup and B.-S. Skagerstam, *Correlations as a handle on the quantum state of the micromaser*, CERN/TH 95-154 preprint, CERN, 1995.
- [27] D. Filipowicz, J. Javanainen and P. Meystre, *The microscopic maser*, Opt. Commun. **58** (1986) 327.
- [28] D. Filipowicz, J. Javanainen and P. Meystre, *Theory of a microscopic maser*, Phys. Rev. **A34** (1986) 3077.
- [29] G. Rempe and H. Walther, *Sub-Poissonian atomic statistics in a micromaser*, Phys. Rev. **A42** (1990) 1650.
- [30] H. Paul and Th. Richter, *Bunching and antibunching of de-excited atoms leaving a micromaser*, Opt. Commun. **85** (1991) 508.
- [31] G. Rempe, F. Schmidt-Kaler and H. Walther, *Observation of sub-Poissonian photon statistics in a micromaser*, Phys. Rev. Lett. **64** (1990) 2783.
- [32] H.-J. Briegel, B.-G. Englert, N. Sterpi and H. Walther, *One-atom maser: statistics of detector clicks*, Phys. Rev. **49** (1994) 2962.

- [33] P. L. Knight and P. W. Milonni, *The Rabi frequency in optical spectra*, Phys. Rep. **66** (1980) 21.
- [34] I. Sh. Averbukh and N. F. Perelman, *Fractional regenerations of wave packets in the course of long-term evolution of highly excited quantum systems*, Sov. Phys. JETP **69** (1989) 464.
- [35] I. Sh. Averbukh and N. F. Perelman, *Fractional revivals: Universality in the long-term evolution of quantum wave packets beyond the correspondence principle dynamics*, Phys. Lett. **A139** (1989) 449.
- [36] M. Fleischhauer and W. Schleich, *Revivals made simple: Poisson summation formula as a key to the revivals in the Jaynes-Cummings model*, Phys. Rev. **A47** (1993) 4258.
- [37] E. M. Wright and P. Meystre, *Collapse and revival in the micromaser*, Opt. Lett. **14** (1989) 177.
- [38] A. M. Guzman, P. Meystre and E. M. Wright, *Semiclassical theory of the micromaser*, Phys. Rev. **A40** (1989) 2471.
- [39] U. Herzog, *Micromasers with stationary non-Poissonian pumping*, Phys. Rev. **A52** (1995) 602.
- [40] J. Krause, M. Scully and H. Walther, *Quantum theory of the micromaser: Symmetry breaking via off-diagonal atomic injection*, Phys. Rev. **A34** (1986) 2032.
- [41] L. Lugiato, M. Scully and H. Walther, *Connection between microscopic and macroscopic maser theory*, Phys. Rev. **A36** (1987) 740.
- [42] K. Zaheer and M. S. Zubairy, *Phase sensitivity in atom-field interaction via coherent superposition*, Phys. Rev. **A39** (1989) 2000.
- [43] W. Schleich and J. A. Wheeler, *Oscillations in photon distribution of squeezed states and interference in phase space*, Nature **326** (1987) 574.
- [44] G. S. Agarwal, *Master equation methods in quantum optics*, in *Progress in Optics XI*, p. 1, Ed. E. Wolf, (North Holland, 1973).
- [45] D. F. Walls and G. J. Milburn, *Quantum optics*, (Springer, 1995)
- [46] G. Rempe, M. O. Scully and H. Walther, *The one-atom maser and the generation of non-classical light*, Physica Scripta **T34** (1991) 5.
- [47] M. C. Teich and B. E. A. Saleh, *Photon bunching and antibunching*, in *Progress in Optics XXVI*, p. 1, Ed. E. Wolf, (North-Holland, 1988).
- [48] L. Mandel, *Sub-Poissonian photon statistics in resonance fluorescence*, Opt. Lett. **4** (1979) 205.
- [49] F.-J. Fritz, B. Huppert and W. Willems, *Stochastische matrizen*, (Springer-Verlag, 1979).

- [50] P. Meystre, G. Rempe and H. Walther, *Very-low-temperature behavior of a micromaser*, Opt. Lett. **13** (1988) 1078.
- [51] P. Filipowicz, J. Javanainen and P. Meystre, *Quantum and semiclassical steady states of a kicked cavity mode*, J. Opt. Soc. Am. **B3** (1986) 906.
- [52] Z. Schuss, *Theory and applications of stochastic differential equations*, (John Wiley and Sons, 1980).